Defining the importance of the arginine loop region of protegrin-1 for antimicrobial activity towards colistin-resistant *Klebsiella pneumoniae.*

Christina DeBarro[a], Sofia Assent[a], Hannah Makhecha[a], Noor Radde[b], Rakesh Krishnan[cdef], Justin Randall[g], Cesar de la Fuente-Nunez[cdef], and Renee M. Fleeman[a]*

[a] Division of Immunity and Pathogenesis, Burnett School of Biomedical Sciences, College of Medicine, University of Central Florida. Orlando, FL 32837

[b] Department of Molecular Biology, The University of Texas at Austin. Austin, TX 78712, USA.

[c] Machine Biology Group, Departments of Psychiatry and Microbiology, Institute for Biomedical Informatics, Institute for Translational Medicine and Therapeutics, Perelman School of Medicine, University of Pennsylvania. Philadelphia, PA 19104, USA.

[d] Departments of Bioengineering and Chemical and Biomolecular Engineering, School of Engineering and Applied Science, University of Pennsylvania. Philadelphia, PA 19104, USA.

[e] Penn Institute for Computational Science, University of Pennsylvania. Philadelphia, PA 19104, USA.

[f] Department of Chemistry, School of Arts and Sciences, University of Pennsylvania, Philadelphia, Pennsylvania, USA.

[g] Department of Biological and Biomedical Systems, University of Missouri-Kansas City. Kansas City, MO 64110, USA.

*Correspondence: Renee.Fleeman@ucf.edu

ORCID account = https://orcid.org/0000-0001-7103-461X

Keywords*: Klebsiella pneumoniae*, antimicrobial peptide, bacterial resistance, genetic screening

Summary

Carbapenem resistant Klebsiella pneumoniae extreme drug resistance has warranted the use of colistin as a last-resort antibiotic but these isolates are now displaying increasing rates of colistin resistance. This is in large part due to the modifications made to the lipid A by the PhoPQ two component system. Host defense peptides (HDPs) are like colistin in that they are both positively charged and display amphipathic character, however are not impacted by lipid A modifications to the extent of colistin. To understand how HDPs can penetrate colistin resistant membranes we performed a deep mutational scanning analysis of protegrin-1 and revealed that amino acids mutations that resulted in alteration of peptide structure had more impact on antimicrobial activity than a reduction in charge. Probing single and double amino acid variants using membrane analysis and molecular modeling revealed the loss of antimicrobial activity correlated with decreased inner membrane leakage and pore modeling predicting decreased pore size,

Introduction

Multidrug-resistant *Klebsiella pneumoniae* is responsible for a wide array of healthcare-associated infections throughout the globe [1-8]. More specifically, as of 2024, the World Health organization has declared carbapenem-resistant *K. pneumoniae* the top priority pathogen [9]. Colistin, a last resort antibiotic, has been used in place of carbapenems to treat carbapenem-resistant *K. pneumoniae* [2, 3, 7, 10-12]. The two *K. pneumoniae* clonal groups most associated with global carbapenem resistance are CG258 and CG15 [3, 13, 14]. While CG15 is more commonly associated with resistance to third-generation cephalosporins, as of 2017 CG258 was responsible for approximately 70% of carbapenem-resistant infections, with cases documented globally [3, 8]. Within this clonal group consists of three sequence types, ST258, ST512, and ST11. Of these sequence types, ST258 has been associated with the majority of carbapenem resistant outbreaks as well as global dissemination of carbapenemases [8, 13, 15, 16]. Importantly, we are now finding an increase in colistin resistance with ST258 clinical isolates [7, 17-20].

Polymyxin B and E (colistin) are cationic cyclic lipopeptides with a charge of +5 that bind to the lipopolysaccharides on the outer membrane of Gram-negative bacteria [10, 21-24]. More specifically, the positively charged diaminobutyric acid residues of colistin bind to the negatively charged phosphate groups on the lipid A portion of a lipopolysaccharide molecule (LPS), displacing the divalent cations already present. This allows the hydrophobic tail of colistin to penetrate the outer membrane, resulting in local membrane curvature. Eventually, colistin will form aggregates within the outer membrane, resulting in structural instabilities. These instabilities allow colistin to cross the lipid bilayer and access the inner membrane. At the inner membrane colistin will cause membrane thinning that will result in cytosolic leakage and bacterial cell death [10, 21-24]. Colistin resistance in *K. pneumoniae* has been largely attributed to the modifications on the outer membrane that alter the charge or structure of the lipid A portion its lipopolysaccharides (LPS) [10, 21-24]. The overall charge of the bacterial membrane can be increased by the replacement of negatively charged phosphates on the lipid A molecule by positively

charged chemical groups such as phosphoethanolamine (PEtN) and 4-amino-4-deoxy-L-arabinose (L-Ara4N) [10, 21-24]. This will reduce colistin's affinity for the bacterial cell due to the disruption of the initial electrostatic interaction. Furthermore, the acyl chains of a lipid a molecule can be altered to increase the rigidity of the bacterial membrane, resulting in the mechanistic expulsion of colistin and thereby resistance [22, 25]. The PhoPQ two-component system has been shown to be a global regulator implicated in colistin resistance in Gram-negative bacteria, including *K. pneumoniae* [26-29]

Host defense peptides are not equally affected by the modifications to the LPS that cause resistance to polymyxins [30-32]. Compared to colistin that directly targets lipid A to displace the stabilizing cations [10, 21-24], host defense peptides interact more generally with the LPS having multiple mechanisms of membrane disruption. These include the 'detergent like' carpet model or the formation of pores through the toroidal pore and barrel-stave models [33-36]. Previous work describing host defense peptide antimicrobial activity towards *K. pneumoniae* revealed that peptides with increased backbone steric hinderance had improved activity, in particular towards colistin-resistant ST-258 *K. pneumoniae* strain MKP103 [37, 38]. This suggests that not all host defense peptides are affected equally by the modifications providing colistin resistance and there are important physiochemical properties that allow them to retain antimicrobial activity towards colistin-resistant Gram-negative pathogens.

Here we describe the investigation into the strong antimicrobial activity of protegrin-1 towards colistin-resistant *K. pneumoniae* MKP103 through a multi-level analysis (**Figure 1**). Deep mutational peptide scanning revealed specific positions necessary for antimicrobial activity in protegrin-1. Furthermore, we found intricate changes to secondary structure could impact antimicrobial activity, while comparatively larger changes to the positive charge of the peptide were needed to impact activity. Specifically, within the triple arginine motif of protegrin-1 a proline mutation decreases antimicrobial activity at position 9 but not at position 11. Mutation of a second arginine residue within this region, regardless of the position of the proline resulted in complete loss of antimicrobial activity. Investigation into the peptide variants

membrane interactions demonstrated changes in cytosolic leakage, which corresponded to the respective activity of our proline peptide variants. Moreover, despite a loss of activity we found an increase in outer membrane disruption with our inactive double mutation peptide variants. Molecular modeling revealed a distinct reduction in diameter and overall pore collapse of the modeled beta-sheet variant octameric pores as well as the rapid loss of beta-sheet character in the variants' monomeric models. These findings challenge the currently set precedent of colistin resistance being largely attributed to differences in charge, where we see with protegrin-1 even with the cysteine bonds in place, intricate changes in structure can impact pore formation in colistin-resistant *K. pneumoniae*.

Results

Host defense peptides do not equally bypass *K. pneumoniae* MKP103 PhoP acquired polymyxin resistance

An increasing number of *K. pneumoniae* isolates are becoming resistant to the last resort antibiotic colistin [7, 17-20]. Colistin is positively charged and displays amphipathic structure, characteristics shared by host defense peptides [21, 39-41]. Host defense peptides are a stressor that is responded to by the PhoPQ two-component system, although the modifications to the LPS causing colistin resistance does not equally apply to all host defense peptides [30-32, 42]. To expand on our understanding of the varying impact of PhoPQ mediated colistin resistance on different host defense peptides first we validated *K. pneumoniae* MKP103 resistance to polymyxins was mediated by upregulation *phoP* and tested the impact of this resistance to antimicrobial activity of different classes of host defense peptides.

To validate PhoPQ mediated polymyxin resistance in *K. pneumoniae* MKP103, we first identified the minimal inhibitory concentration (MIC) of polymyxin B and colistin (polymyxin E) next to other well published *K. pneumoniae* strains. We found minimal polymyxin resistance with hypervirulent *K. pneumoniae* NTUH [43] and KPPR1S [44], drug-resistant *K. pneumoniae* ATCC 700603 [45], and type strain *K. pneumoniae* ATCC 13883 [46] (MICs < 1 μmol L^{-1}) when compared to *K. pneumoniae* MKP103, a genetically modified ST-258 strain used for the creation of a transposon library (MIC 27 μmol L^{-1}) [47, 48] (**Table S1, Figure 2A**). We then determined the baseline expression levels of response regulator *phoP* with RT-qPCR to compare to their respective polymyxin resistance [49, 50] and found high levels of *phoP* expression correlated with colistin resistance in *K. pneumoniae* MKP103 (**Figure 2A,Figure S1**). Therefore, we determined *K. pneumoniae* MKP103 to be the ideal screening candidate for our investigation into PhoPQ mediated colistin resistance.

To determine a candidate host defense peptide for our deep mutational scanning, we used the parental MKP103 and its *ΔphoP* transposon mutant (KPNIH1_10030-701::T30) and compared MICs of different

125 structural classes of antimicrobial peptides (**Table 1**). As shown with previous studies on colistin
126 resistance [30-32], we found that PhoP mediated polymyxin resistance does not extend equally to host
127 defense peptides compared to polymyxin B and E, which had a 256-fold change between the parental
128 strain and *ΔphoP* mutant (**Figure S1, Figure 2B**). Specifically, the largest fold change in MIC between
129 the parental strain and *ΔphoP* mutant was with indolicidin (16-fold), an extended host defense peptide
130 with a random coil structure (**Figure 2B**). Furthermore, when testing alpha-helical peptides, we saw LL-
131 37 and melittin (8-fold change MIC) were similarly affected by PhoP mediated resistance while cecropin
132 A was slightly less affected (4-fold change MIC). When testing beta-sheet peptides, protegrin-1 and
133 arenicin both had a 4-fold change in MIC between the parental strain and *ΔphoP* mutant. Finally, as
134 expected due to its internal mechanism of killing [51], the polyproline peptide bac7 (1-35) had only 2-fold
135 change in MIC between the MKP103 parental strain and *ΔphoP* mutant. For a comparison of the peptide
136 backbone steric hindrance of the tested host defense peptides following up on previously observed
137 finding [37], we created Ramachandran plots of the host defense peptides displaying the dihedral rotation
138 angles of each amino acid residue. The alpha helical host defense peptides (ll-37, cecropin, and melittin)
139 plotted within the right-handed alpha-helical region of the Ramachandran plot (**Figure 2C**) revealing the
140 precise angles needed to form a helical protein [52-54] due to the flexibility of the peptide backbone. The
141 beta-sheet peptides (protegrin-1 and arenicin) and extended peptides (bac7 (1-35) and indolicidin) plotted
142 within the beta-sheet/collagen triple helix region of the Ramachandran plot (**Figure 2D, and 2E**), a region
143 known for being the most restrictive for amide bond rotation [54]. Although indolicidin localized within this
144 region, the individual amino acids displayed a range of flexibility, shown by the spread on the
145 Ramachandran plot. Collectively, host defense peptides that had tight localization to the beta-
146 sheet/collagen triple helix region of the Ramachandran plot were less impacted by *K. pneumoniae*
147 MKP103 PhoP mediated colistin resistance. Protegrin-1, along with having a low fold change between
148 parental MKP103 and *ΔphoP* mutant, also has a well characterized structure and mechanism of action
149 [55-57]. Furthermore, this peptide's two disulfide bonds, which are responsible for protegrin-1's tightly

150 constraint structure, are ideal for molecular dynamic simulations [58]. For these reasons we chose this
151 peptide as our candidate for deep mutational scanning to investigate the ability of this host-defense
152 peptides to bypass *K. pneumoniae* colistin resistance.
153

154 **Protegrin-1 deep mutational scanning library shows reveals charge and structure are important**
155 **for antimicrobial activity towards colistin-resistant *K. pneumoniae* MKP103**

156 To understand the importance of individual amino acids to the antimicrobial activity of beta-sheet peptide
157 towards colistin-resistant *K. pneumoniae* we next aimed to perform deep mutational scanning analysis of
158 the beta-sheet peptide protegrin-1. For this we utilized the Surface Localized Antimicrobial Display
159 (SLAY) system that was designed to display antimicrobial peptides on the surface of Gram-negative
160 bacteria to capitalize on the high-throughput advantages of next-generation sequencing [59]. Further
161 optimization of this platform led to the development of deep mutational scanning with SLAY (dmSLAY),
162 using this tool to assess protegrin-1 and describe features driving membrane selectivity between bacteria
163 and mammalian cells [60]. As previously described, the creation of the protegrin-1 dmSLAY ensured a
164 high level of conservation was given to the mixed base primer sequence (**Table S2, Figure S2**), with the
165 possibility of 7-12 changes at each amino acid residue, resulting in 1-9 mutations per peptide variant. We
166 aimed to expand on this impactful study by testing the protegrin-1 dmSLAY library in colistin-resistant *K.*
167 *pneumoniae* MKP103.

168

169 We collected the plasmid-based library from colistin-resistant *K. pneumoniae* MKP103 following growth
170 for four hours with and without plasmid induction with isopropyl β-D-thiogalactoside (IPTG). To predict
171 antimicrobial activity of the peptide variants in our library, we used next generation sequencing to quantify
172 the plasmids from the induced versus the uninduced population **(Table S3)**. Sequences that express for
173 an active peptide variant are removed from the population of plasmids following induction resulting in a

174 negative log2 fold change in reads. With the goal to understand what amino acids were implicated in
175 retaining the antimicrobial activity of protegrin-1, we looked for retention within the population of peptide
176 variants rather than removal and used a log2 fold change value of 0 or higher is indicative of lack of
177 antimicrobial activity. Overall, we identified approximately 1700 peptide sequence variants lacking activity
178 against *K. pneumoniae* MKP103 **(Figure 3A; Supplemental data file 1).** To determine which specific
179 amino acid residues were necessary to bypass colistin resistance, we chose to investigate individual
180 mutations that occurred most often in our inactive peptide variant population, rather than testing peptide
181 variants from the screen **(Table S4)**. We had some individual amino acid mutations that occurred only
182 ≤20 peptide variants. However, we were intrigued to find several amino acid mutations that were in the
183 majority of peptide variants retained in the population **(Table 2, Figure 3B).** We chose not to investigate
184 mutations with less than 25 occurrences, those that did not involve an amino acid class change, and
185 those that impacted disulfide bonds, as literature has already shown their importance for protegrin-1's
186 antimicrobial activity [61, 62]. This resulted in the selection of five individual mutations in different
187 structural regions of protegrin-1 to investigate their effects alone on the surface display system (**Figure**
188 **3B**). Specifically, the glycine at position to mutated to an arginine (G2R) increasing the charge of the
189 unstructured tail region was found 316 times within the population of peptide variants that had a log2 fold
190 change >0. A leucine mutation to an isoleucine (L5I) and phenylalanine to leucine (F12L) within the beta-
191 sheet region were found in 218 and 834 of peptide variants retained in the population, respectively.
192 Finally, we found mutations in 2 arginine residues of the triple arginine loop region (R9P and R10L) times
193 295 and 299 within the population of peptide variants retained in the population, respectively and these
194 variants most often occurred together.

195

196 To test the selected individual mutations using the SLAY platform, we cloned the single amino acid
197 variants of protegrin-1 into the genetic screening system **(Table S5, S6)** and induced the plasmid in
198 colistin-resistant *K. pneumoniae* MKP103 over a four-hour period enumerating CFU mL^{-1}. When testing

199 the parental peptide displayed on the surface with 1 mM IPTG induction we found there was a 5-log
200 reduction in CFU mL^{-1} when compared to an uninduced plasmid control, and bacteria harboring the
201 system with a tandem influenza hemagglutinin peptide (2xHA) as a negative control **(Figure 3C)**. Testing
202 the individual amino acid mutations next to the parental peptide, we found the mutation of an arginine to
203 leucine (R10L), glycine to arginine (G2R), leucine to isoleucine (L5I), and phenylalanine to leucine (F12L)
204 mutations displayed minimal change in CFU mL^{-1} compared to the surface display of the parental peptide
205 (**Figure 3D).** However, when introducing a proline mutation at position 9 (R9P), we saw this single
206 mutation could reduce the activity of the peptide towards colistin-resistant *K. pneumoniae* MKP103 by 2-
207 fold compared to our parental peptide**.** Intriguingly, we found the arginine to proline mutation in our next-
208 generation sequencing occurred approximately 89% of the time with an arginine to leucine mutation at
209 position 10 (R9P, R10L). Therefore, we also tested these amino acid mutations together using SLAY and
210 found the complete loss of activity of the peptide with two arginine amino acid residues mutated within
211 the triple arginine motif (**Figure 3D**). Overall, our deep mutational scanning of protegrin-1 identified
212 candidate amino acids that are important for antimicrobial activity towards colistin-resistant *K.*
213 *pneumoniae.* Although many of these mutations needed additional mutations for a reduction in
214 antimicrobial potential, we identified a single arginine to proline mutation at position 9 within the beta-
215 sheet to turn transition region of the triple arginine motif that alone could impact antimicrobial activity and
216 the complete loss of activity when this was accompanied by a second mutation within this region.

217

218 **The arginine to proline mutation impedes antimicrobial activity only in the beta-sheet to turn**
219 **transition region of the protegrin-1 arginine loop**

220 With the intriguing findings from our deep mutational scanning of protegrin-1 arginine loop beta-sheet to
221 turn transition region, we had the single (R9P and R10L) and double (R9P, R10L) protegrin-1 variants
222 synthesized to test their antimicrobial activity towards of *K. pneumoniae* MKP103 parental strain next to

223 the *ΔphoP* mutant, mutants downstream of PhoP regulon, and a panel *K. pneumoniae* clinical isolates.
224 In addition to testing amino acids discovered in our dmSLAY analysis, we also synthesized a single and
225 double variant with a proline mutation at position 11 (R11P and R10L, R11P). This placed the proline
226 amino acid substitution within the peptide's turn region rather than its beta-sheet to turn transition region
227 **(Table 3)** and test the importance of the changes to peptide positive charge versus the secondary
228 structure that were introduced by the R9P mutation. Furthermore, in order to investigate the position itself
229 rather than the amino acid mutation found in that position, we also synthesized alanine and lysine single
230 peptide variants at positions 9 (R9A and R9K) and 11 (R11A and R11K).

231 When testing antimicrobial activity towards the colistin-resistant *K. pneumoniae* MKP103 used for
232 screening, both the R9P and R10L variant displayed a reduction of activity compared to protegrin-1 (MIC
233 15.23 and 15.11 μmol L^{-1}, respectively) **(Table 4)**. We observed that despite a reduction in charge (charge
234 +5), the R11P variant retained the same level of antimicrobial activity toward our colistin-resistant isolate
235 as protegrin-1 (charge +6) (MICs 3.8 μmol L^{-1} respectively). When testing the double mutant variants
236 (R9P, R10L and R10L, R11P) (charge +4), we found they both lost activity towards *K. pneumoniae*
237 MKP103 (MIC >30 μmol L^{-1}). Interestingly, when substituting either position 9 or 11 with an alanine (R9A
238 or R11A) we found the similar antimicrobial activity to the R9P peptide variant (MICs 15.41,15.41, 15.23
239 μmol L^{-1}, respectively). However, when substituting position 9 and 11 with a lysine (R9K or R11K) we
240 have smaller changes in activity, indicating charge retention at these positions has variable impacts on
241 antimicrobial activity (MICs 3.75 and 7.50 μmol L^{-1}, respectively).

242

243 To broaden the impact of our findings beyond *K. pneumoniae* MKP103 we selected colistin-resistant
244 clinical isolates from the Mult-drug-Resistant Organism Repository and Surveillance Network (MRSN) *K.*
245 *pneumoniae* diversity panel to test the peptide variants against [63]. We found although the majority of
246 isolates (64 MRSN isolates) were colistin sensitive (MIC ≤ 0.87 μmol L^{-1}), there were 31 isolates that

247 displayed moderate colistin resistance (MIC 1.73-6.92 μmol L^{-1}), and 5 isolates (MRSN 13768, 430414,
248 430405, 560539, and 728987) that displayed elevated colistin resistance (MICs >13 μmol L^{-1}) **(Table S7)**.
249 Of note, two isolates, MRSN 13768 and 430414, had colistin MICs comparable to that of *K. pneumoniae*
250 MKP103 (27.69 μmol L^{-1}). However, when assessing our protegrin-1 peptide variants towards these
251 clinical isolates, we found that majority our MICs were relatively similar to the parental peptide protegrin-
252 1, with the R9P single variant displaying the least antimicrobial activity (3.81 μmol L^{-1}) (**Figure 4A**). When
253 testing the double mutant variants (R9P, R10L and R10L, R11P) we found they lost antimicrobial activity
254 towards 3 of the 5 colistin resistant MRSN clinical isolates. Specifically, MRSN 430405 (colistin MIC 27.69
255 μmol L^{-1}), was completely resistant to the beta turn double mutant peptide variant (R10P, R11L MIC 31.09
256 μmol L^{-1}) but not the beta sheet double variant (R9P, R10L MIC 7.77 μmol L^{-1}). Furthermore, MRSN
257 560539 (colistin MIC 13.85 μmol L^{-1}) displayed the same level of resistance to both beta sheet and beta
258 turn double variants (MICs 15.54 and 15.55 μmol L^{-1}, respectively) and MRSN 728987 (colistin MIC 13.85
259 μmol L^{-1}) was slightly more sensitive to the double mutant peptide variants (MIC 7.77 μmol L^{-1}).

260

261 When assessing the changes in MIC in the absence of PhoP regulon induction using the *ΔphoP* mutant,
262 we found the beta sheet peptide variants (R9P and R9P, R10L) had a larger fold-change in antimicrobial
263 activity between the mutant and parental *K. pneumoniae* MKP103 than the beta turn variants (R11P and
264 R10L, R11P) **(Figure 4B)**. Of note, when comparing this the parental peptide protegrin-1, we found the
265 beta sheet peptide variants (R9P and R9P,R10L) displayed the same 32-fold decrease in MIC toward
266 the *ΔphoP* mutant as protegrin-1, whereas the beta turn peptide variants (R10L, R11P, and R10L, R11P)
267 only displayed an 8-, 4-, and 8-fold decrease in MIC towards the *ΔphoP* mutant, respectively.
268 Furthermore, we tested *K. pneumoniae* MKP103 transposon mutants of downstream genes within the
269 PhoP regulon, involved in modifying either the rigidity or charge of the LPS [25, 42]. Specifically, PagP
270 transfers a palmitate group to a lipid A molecule and PagL removes an acyl group, altering the

271 membrane's fluidity and permeability [25, 64], while ArnT and PmrB are involved in the addition of a 4-
272 amino-4-deoxy-L-arabinose (L-Ara4N) on lipid A, increasing the positive charge of the outer membrane
273 [25]. We found no difference between the MICs of parental protegrin-1, the beta sheet peptide variants
274 (R9P and R9P, R10L), indicating a combination of LPS modifications are necessary for the sensitivity
275 displayed by the *ΔphoP* mutant (**Figure 4B**). Interestingly, although the beta turn peptide variants did not
276 show as much of a fold-change in MICs with the *ΔphoP* mutant as the beta sheet peptide variants and
277 parental peptide protegrin-1, we found a slight fold-change increase in MIC between the downstream
278 PhoP regulon mutants compared to the parental *K. pneumoniae* MKP103. Specifically, when testing the
279 R11P variant, the *ΔpagL and ΔpagP* transposon mutants (KPNIH1_07455-208::T30 and KPNIH1_13050-
280 101::T30, respectively) displayed 4-fold decrease in MIC (MIC 0.96 μmol L^{-1}) **(Table S5)** compared to *K.*
281 *pneumoniae* MKP103 (MIC 3.81 μmol L^{-1}), while the *ΔarnT and ΔpmrB* transposon mutants
282 (KPNIH1_24880-114::T30 and KPNIH1_08200-303::T30) displayed 2-fold decrease in MIC (MICs 1.90
283 μmol L^{-1}). Finally, the beta turn double mutant peptide variant (R10L, R11P) all four PhoP regulon
284 transposon mutants displayed a 2-fold increase in MIC.

285

286 Upon investigation of positions 9 (beta sheet) and 11 (beta turn) within protegrin-1 with alanine and lysine
287 amino acid substitutions, we find much more variability within our colistin resistant clinical isolates than
288 the mutations that came from the dmSLAY analysis of *K. pneumoniae* MKP103 **(Figure 4C)**. Specifically,
289 alanine substitution at position 9 (beta turn) had MICs of 15.42 and 30.84 μmol L^{-1} towards MRSN 13768
290 (colistin MIC 27.79 μmol L^{-1}) and MRSN 430505 (colistin MIC 13.85 μmol L^{-1}), respectively. MRSN
291 430505 also displayed higher resistance towards the peptide variant with alanine substituted in the turn
292 region (R11A MIC 15.00 μmol L^{-1}) and lysine substituted in the sheet region (R9K MIC 15.42 μmol L^{-1}).
293 These peptides also displayed less variability between the antimicrobial activity towards the parental
294 strain *K. pneumoniae* MKP103 and the PhoPQ regulon transposon mutants. Contrary to our variants

295 identified from the initial screening, we found increased fold change in activity between the parental strain
296 and PhoP regulon transposon mutants **(Figure 4D)**. Interestingly, we see these less bulky substitutions
297 at position 11 variants (R11A, R11K) were more impacted by the downstream individual PhoP regulated
298 changes than the position 9 variants (R9A, R9K). Specifically, R11A peptide variant when tested against
299 the *ΔpagP, ΔpagL, and ΔarnT* transposon mutants resulted in a 16-fold decrease in MIC compared the
300 parental strain, and *ΔpmrB* transposon mutant had an 8-fold lower MIC. When testing our peptide variants
301 against other Gram-Negative bacteria we find that regardless of variant, *Burkholderia thailandensis* [65]
302 exhibits complete resistance, while *Acinetobacter baumannii* [66] and both *Escherichia coli* [60, 67, 68]
303 strains display high sensitivity to all peptide variants, suggesting these peptide variants identified in this
304 study are unable to bypass Gram-negative bacteria with high levels of colistin resistance **(Table S8)**.
305 Collectively, we found when proline was introduced to the turn region (R11P) of the triple arginine motif
306 had less impact on the antimicrobial activity than when placed in the beta-sheet to turn transition region
307 (R9P) and that removing an additional arginine from the triple arginine motif regardless of the proline
308 position completely abolished antimicrobial activity towards colistin-resistant *K. pneumoniae* MKP103.

309

310 **Protegrin-1 double mutant variants with reduced charge display greater disruption of colistin-**
311 **resistant outer membrane**

312 We found modifications to the outer membrane LPS by the PhoP regulon increase resistance to our beta
313 sheet peptide variants more than our beta turn variants, indicating a role in that amino acid in bypassing
314 colistin resistance LPS modifications. Furthermore, we found a dichotomy between colistin resistance
315 and peptide variant resistance when testing the MRSN clinical isolates, where the moderately elevated
316 colistin resistant clinical isolates (MIC 1.73-6.92 μmol L^{-1}), are more resistant to the double mutant peptide
317 variants compared to the more colistin resistant clinical isolates (MIC 13 μmol L^{-1}). Therefore, when
318 assessing the mechanism of action of the peptide variants compared to the protegrin-1 parental peptide,
319 we wanted to first probe the outer membrane integrity following treatment as protegrin-1 must interact

320 and bypass the outer membrane before forming a pore at the inner membrane. To evaluate changes in
321 outer membrane permeability, we used N-Phenyl-1-naphthylamine (NPN), a hydrophobic small molecule
322 impermeable to an intact outer membrane that fluoresces weakly with increased fluorescence observed
323 upon outer membrane disruption [69-71].
324
325 When testing the parental strain *K. pneumoniae* MKP103, our single point mutations (R9P, R10L and
326 R11P) at 31 μmol L^{-1} behave similarly to protegrin-1 but also polymyxin B (MIC 27 μmol L^{-1}) **(Figure 5A).**
327 Unexpectedly, the double mutation variants (R9P, R10L and R10L, R11P) when tested at 31 μmol L^{-1}
328 display higher fluorescence of NPN than parent protegrin-1, indicating increased disruption of the outer
329 membrane of colistin-resistant *K. pneumoniae* MKP103 **(Figure 5B).** Interestingly, when testing our
330 *ΔphoP* mutant **(Figure 5C and 5D)** and downstream mutants modifying both charge and fluidity, all
331 peptide variants display higher fluorescence of NPN (**Figure S3)**. Our beta sheet double peptide variant
332 in these cases had activity similar to or less than our parent peptide. Comparing the endpoint
333 fluorescence across isolates we find the least amount of disruption from our single mutant peptide
334 variants with our *ΔpagL* transposon mutant **(Figure 5E)**. We also find that in every isolate our more active
335 variant (R11P) is less effective at disrupting the outer membrane compared to our less active variant
336 (R9P). When observing endpoint fluorescence of our double mutant variants we also see the least
337 amount of disruption with our *ΔpagL* transposon mutant **(Figure 5F)**. When testing our most colistin
338 resistant clinical isolates, the peptide variants also display higher fluorescence of NPN **(Figure S4)**.
339 However, our beta turn double peptide variant (R10L, R11P) disrupts the outer membrane more
340 effectively than the beta sheet double peptide variant (R9P, R10L) **(Figure S4)**. Overall, we account for
341 some but not all of the changes in antimicrobial activity towards parental MKP103 with differences in
342 peptide interactions within the outer membrane.
343

344 **The arginine to proline mutation in the beta-sheet transition limits cytosolic leakage in single and**
345 **double mutation variants**
346 Protegrin-1 has a membrane disruptive mechanism of action and has been described to form pores in
347 the inner membrane of the bacteria [55, 72]. To assess the peptide variants loss of membrane disruptive
348 killing, we investigated their ability to depolarize and cause leakage of the inner membrane of colistin-
349 resistant *K. pneumoniae* MKP103. Depolarization is caused by many host defense peptides including
350 those that do not form pores [73, 74]. However, predominantly pore forming peptides can cause leakage
351 of the cytoplasmic components [75, 76]. With the lesser degree of outer membrane disruption observed
352 with our more active peptide variants, we hypothesize they are penetrating to the inner membrane but
353 their mechanism of interaction with the inner membrane is variable depending on the mutations
354 introduced. We evaluated changes in membrane polarity across the inner membrane with 3,3'-
355 dipropylthiadicarbocyanine Iodide ($DiSC_3$) [77]. This cationic dye inserts into polarized inner membranes
356 quenching its fluorescence and depolarization of the inner membrane results in release of the dye and
357 an increase in fluorescence. When testing the single mutation variants (R9P, R10L and R11P) at 31 μmol
358 L^{-1}, only our beta sheet single peptide variant (R9P) depolarized the inner membrane of resistant *K.*
359 *pneumoniae* MKP103 to the extent of the parent protegrin-1, while our more active beta turn variant
360 (R11P) depolarized the inner membrane less than our parent peptide **(Figure 6A)**. Our less active beta
361 turn variant (R10L) comparatively exhibited the least amount of depolarization toward MKP103. When
362 testing the double mutation peptide variants (R9P, R10L and R10L, 11P) at 31 μmol L^{-1}, both variants
363 depolarized the inner membrane less than the parent protegrin-1 **(Figure 6B)**. Overall, all peptide variants
364 depolarized the inner membrane greater than the polymyxin B, tested at 31 μmol L^{-1}. We continued our
365 investigation of changes in inner membrane polarity with our *ΔphoP* transposon mutant. We found that
366 unlike our parental isolate, both our R9P and R11P depolarize the inner membrane to the same extent
367 as parent protegrin-1 **(Figure 6C)**. Our beta turn single variant (R10L) does continue to have the lowest
368 depolarization ability of all our peptide variants. This trend continues with our double variants, where both

369 our beta turn and beta sheet double variants exhibit depolarization on par with our parent peptide **(Figure**
370 **6D)** rather than lower depolarization, as seen in our parent MKP103.
371
372 To assess for changes in cytoplasmic leakage, we utilized ortho-nitrophenyl-β-galactoside (ONPG), a
373 substrate that is hydrolyzed to ortho-nitrophenol (ONP) by cytoplasmic β-galactosidase [78]. When
374 testing the single mutation peptide variants (R9P and R11P) at 31 μmol L^{-1} , we found although both
375 variants resulted in leakage similar to the parental protegrin-1, there was a delay in the time to cause
376 equal leakage (**Figure 7A**). Specifically, the R11P peptide variant matched the ONP levels induced by
377 the parental protegrin-1 after 25 minutes, while the R9P peptide variant did not match the leakage until
378 40 minutes. Surprisingly, our beta turn single variant (R10L) resulted in very little inner membrane
379 leakage, displaying levels less than our inactive polymyxin B. When testing the double mutation variants
380 (R9P,R10L and R10L,R11P) at 31 μmol L^{-1}, our beta sheet double peptide variant resulted in a decrease
381 in the ONP levels compared to the parental protegrin-1 and displayed levels similar to the inactive
382 polymyxin B (**Figure 7B**). The beta turn double peptide variant displayed a delay in fluorescence
383 compared to the parental protegrin-1 at this concentration **(Figure 7B)**. Investigation with our *ΔphoP*
384 transposon mutant resulted in an overall inability to effectively disrupt the inner membrane with all peptide
385 variants **(Figure 7C and D)**. We also find that all peptide variants behave similarly to parent protegrin-1
386 regardless of differences in antimicrobial activity. Our beta turn single variant (R10L), however, still
387 behaves similarly to our inactive polymyxin B. **(Figure 7C)**. Collectively, our results show that all peptide
388 variants depolarize the inner membrane but changes in cytoplasmic leakage correlate best with the
389 peptide variants MICs.
390
391 **Molecular modeling shows octameric pore collapse and loss of beta sheet character in beta sheet**
392 **peptide variants.**

393 We found the membrane leakage to correspond to the decrease in antimicrobial activity observed with
394 our peptide variants suggesting a deficiency in the pore formation potential of the peptide variants. Alpha
395 helical peptides like ll-37 have been shown to dimerize before insertion into the membrane [79]. However,
396 protegrin-1 has been shown to dimerize within the phospholipid bilayer of the inner membrane ultimately
397 leading to octameric pore formation [55]. Therefore, to provide a full spectrum of the potential of the
398 mutations in the peptide variants we modeled the peptide variants before and after interaction with the
399 bacterial membrane, as well as their octameric pore conformations when fully inserted. We also chose
400 to eliminate our beta turn single peptide variant (R10L) due to its inability to cause any inner membrane
401 leakage.

402

403 We modeled our octameric pores utilizing AlphaFold2 with the sequences aligned in the N- to C-termini
404 direction. Images were visualized and diameter distances generated utilizing ChimeraX. Compared to
405 our parent peptide **(Figure 8A)**, our less active single peptide variant (R9P) **(Figure 8B)** exhibits a
406 reduction in diameter in our octameric pore model (~20Å to 11Å, respectively). In contrast, our more
407 active single peptide variant (R11P) **(Figure 8C)** changes the orientation of the hypothetical pore but
408 maintains pore diameter at ~20Å. When comparing our parent peptide to our double peptide variants we
409 find our beta sheet double peptide variant (R9P, R10L) also exhibiting a pore reduction **(Figure 8D)** to
410 ~14-15 Å, and our beta turn double peptide variant (R10L, R11P) **(Figure 8E)** maintained the pore
411 diameter (~ 18Å). This suggests that perhaps the monomeric structures involved in pore formation are
412 differentially impacted by our introduced mutations.

413

414 To better understand the peptide variants behavior within the octameric pore, we modeled our peptide
415 as monomeric subunits and observed how the structure of the peptide became altered in solution. To do
416 this we utilized GROMACS, a molecular dynamics software that uses different algorithms to model the

behavior of the peptide and its interactions with individual molecules over a span of time. These mutations were modeled in an environment of 0.15M NaCl at 310K over the course of 100ns to observe changes in the structural conformation of each peptide mutant [80]. We use Secondary Structure Predictors (DSSP) to observe changes in beta-sheet character over the simulation period. Compared to the parent peptide **(Figure 8F)**, the proline mutation at position 9 resulted in a shortened beta-sheet in its initial structure and an early loss of beta sheet character, at approximately 4000 frames (40 ns) that was never regained throughout the simulation **(Figure 8G)**. However, at position 11, the initial structure remained close to that of the parent peptide and the loss of beta character occurred after the halfway point of the simulation, at approximately 60000 frames (60 ns) (**Figure 8H).** When assessing the double peptide variants, the beta sheet region variant (R9P, R10L) does display a minor level of beta-sheet character throughout the simulation, however it is interwoven with regions of disorder. Furthermore, its initial structure does have shorter beta sheets when compared to the parent peptide **(Figure 8F and 8I).** Finally, our beta turn double peptide variant, (R10L, R11P) results in no changes to its initial structure when compared to the parent peptide. This double mutation fully loses its beta sheet character at approximately 60000 frames (60 ns) and regains it at approximately 80000 frames (80 ns), which may account for its ability to form a correctly oriented pore **(Figure 8E and 8J)**.

Protegrin-1 dimerizes before aggregating into an octameric pore inside the inner membrane. To better assess how our mutations altered peptide structure we assessed changes in its ability to form a dimer. Once again, we utilized GROMACs and an environment of both 0.15M NaCl at 310K and a general Gram-Negative inner membrane, over the course of 100ns [80, 81]. Before and after snapshots were taken to observe changes in the secondary structure of each mutated dimer compared to the parent **(Figure 8K)**. Parent protegrin-1 does not seem to align itself as a dimer in the salt box at the beginning or end of the simulation. This is also true in the Gram-Negative inner membrane simulation where it overlaps at the beta turn region at the beginning and orients across from itself after 100ns. This is unlike both single peptide variants **(Figure 8L and 8M)**. Both align themselves together at the beginning of the simulation.

Our R9P only aligns one beta sheet at the end of the simulation, however, it does display a lengthened beta-sheet. This is unlike R11P, which does not display a lengthened beta sheet at the end of the simulation. Inside the Gram-Negative environment, both single mutant variants orient very similarly at the beginning of the simulation, however at the end they orient themselves diagonally in opposing directions. Our beta sheet double peptide variant found in the screen (R9P, R10L) also aligns with itself at the beginning of the simulation and displays some alignment towards the end **(Figure 8N)**. Our other beta turn double peptide variant, R10L, R11P also aligned itself at the beginning of the simulation **(Figure 8O)**. Unlike all the other mutations, however, there is no alignment at the end of the simulation. In the Gram-negative inner membrane model, both double peptide variants exhibit diagonal alignment of both of their beta sheets, albeit in opposing directions. Looking at how each dimer behaves over the course of the simulation, protegrin-1 has a larger and more variable center of mass than all our point mutations, suggesting a less stable conformation **(Figure S5A)**. Our mutated peptide variants all behaved similarly, having a lower center of mass compared to the parent peptide. This suggests less movement and could explain why there was partial alignment of the peptide variants in the salt environment after 100ns **(Figure 8K-O)**. Furthermore, there were fewer contacts that existed between the dimers of parent protegrin-1 over the course of the salt box simulation **(Figure S5B)**. Meaning this set of monomers were not interacting with each other, explaining why there is no alignment at the end of the simulation **(Figure 8K-O).** Aside from our RR910PL point mutations, all other mutations have a larger and about the same number of contacts across the simulations. Our RR910PL mutation had two instances of a higher number of contacts, from approximately 4000 to 6000 ns, and 8000 to 8500 ns. This change in the number of contacts may explain its change in alignment compared to our other point mutations. Within the context of our Gram-negative inner membrane simulation our parent peptide also exhibited a large center of mass compared to our peptide variants, which could explain why at the end of the simulation they look as if on opposing sides of a potential pore **(Figure 8K, S5C)**. Furthermore, there is a decrease in the number of contacts between each chain over the course of the simulation **(Figure S5D)**. However, unlike in our salt box there is a much larger gap in the initial number of contacts. This could be due to how they initially

469 intercalated within the inner membrane bilayer. Taken together these hypothetical models show our
470 peptide variants with beta sheet (R9P and R9P, R10L) mutations impact pore formation and our
471 monomeric subunits exhibit a rapid loss of beta sheet character not seen with our beta turn variants
472 (R11P and R10L, R11P).
473
474

475 **Discussion**

476 Carbapenem *K. pneumoniae* resistant isolates are now acquiring resistance to the last resort antibiotic
477 known as polymyxin E or colistin [7, 17-20]. This resistance is attributed to modifications to the LPS by
478 the PhoPQ two component system [26-29]. Here we corroborate previous literature stating that host-
479 defense peptides are not equally affected by these LPS modifications as colistin [30-32,37,38], especially
480 protegrin-1 **(Figure 2B)**. The absence of resistance, combined with its well characterized structure and
481 robust antimicrobial activity [54-56] made protegrin-1 an ideal candidate to investigate colistin resistance
482 in *K. pneumoniae.*

483

484 Utilizing our dmSLAY genetic screening platform in combination with quantitative next generation
485 sequencing we found five amino acid mutations that were abundant in the population of plasmids retained
486 following 4-hour induction, indicating they may alter the antimicrobial activity of protegrin-1. First, an
487 arginine substituting a glycine (G2R) in the tail region, potentially altering charge localization of the
488 peptide to the point where it no longer retained activity. An isoleucine substituting a leucine (L5I) in the
489 first beta-sheet potentially adding more bulk to the peptide. A proline in the triple arginine motif within the
490 beta-sheet to turn transition (R9P) that could introduce a kink and potentially disrupting the function of
491 the peptide. Finally, a leucine in both the turn region (R10L) and second beta-sheet (F12L) that would
492 allow for less binding of the peptide when compared to an arginine or phenylalanine, respectively. We
493 also found that our beta sheet proline and beta turn leucine mutations (R9P, R10L) most commonly
494 occurred together in peptide variants retained within the population. To test the effects of these mutations
495 independently without other peptide modifications, we directly cloned them into our surface display
496 genetic platform and performed growth analysis, revealing the beta sheet region arginine to proline (R9P)
497 and beta turn region arginine to leucine (R10L) mutations has the greatest impact on the antimicrobial
498 activity of protegrin-1, and combining these mutations (R9P,R10L) resulted in a complete loss of
499 antimicrobial activity **(Figure 3D)**. Overall, we were surprised that more mutations resulted in possible
500 structural changes rather than changes to charge in the population retained in the population in the

501 dmSLAY analysis, because charge has been the major factor shown to contribute to bypassing the Gram-
502 negative membrane [82]. This included those that added arginine residues to the unstructured tail region
503 (G2R and G3R) increasing the charge of the peptide but not antimicrobial activity.
504
505 We then synthesized peptide variants to validate the surface display system and test our hypothesis that
506 structure potentially supersedes charge. Specifically, we synthesized R11P and R10L,R11P peptide
507 variants that placed the proline residue in the turn region of the triple arginine motif rather than the beta
508 sheet transition region. We found then when testing these variants against MKP103 that our R11P
509 peptide variant retains antimicrobial activity and our R9P peptide variant loses activity, despite a charge
510 reduction on +1 in both peptide variants **(Table 4)**. Furthermore, when comparing the activity of our
511 peptide variants against MKP103 and transposon mutants of genes under the regulation of PhoP, we
512 find the fold change difference in activity is lower with our variants in the beta turn region versus the beta
513 sheet region **(Figure 4B)**. These modifications both resulted in a loss of charge but did not equally lose
514 antimicrobial activity, challenging the paradigm that charge is not necessarily most important aspect in
515 the ability of host defense peptide ability to overcome colistin resistance. To further test this hypothesis,
516 we tested the addition of alanine and lysine modifications to positions 9 and 11 on protegrin-1.
517 Surprisingly, we found these smaller amino acids when substituted at position 11 (R11A and R11K)
518 resulted in a less antimicrobial activity towards colistin-resistant *K. pneumoniae* and this activity is
519 rescued when testing mutants of colistin resistance modifying genes. These findings reinforce our
520 hypothesis that small changes to structure, not just the loss of the cystine residues can impact
521 antimicrobial acidity of protegrin-1 more than a +1-charge reduction.
522
523 To understand the changes in activity observed with the synthesized peptide variants, we investigated
524 their interactions with the outer and inner bacterial membrane. Outer membrane permeability accounted
525 for some of our activity changes as both our double variants exhibited higher fluorescence compared to
526 the parent peptide, suggesting they are getting stuck within the outer membrane **(Figure 5A)**. This is in

527 line with what has been shown with polymyxin B nonapeptide lacking the lipid tail that can still increase
528 penetration through the outer membrane without inner membrane lysis [83]. The differences in
529 antimicrobial activity between our single proline peptide variants (R9P and R11P) correlated will with
530 inner membrane permeability. We found R9P peptide variant exhibited a slower accumulation of inner
531 membrane leakage compared to R11P, which behaved similarly to the parent peptide **(Figure 7A),**
532 revealing changes in pore formation ability may be the reason for the decrease in antimicrobial activity
533 with the R9P peptide variant. These findings reveal the small changes to protegrin-1 structure, not just
534 the major changes observed with cysteine bond removal [62], can impact inner membrane leakage of
535 the colistin-resistant *K. pneumoniae* membrane.
536
537 At the inner membrane protegrin-1 forms octameric pores, which cause cytoplasmic leakage [55].To
538 understand why our peptide variants behaved differently at the inner membrane we modeled our variants
539 as octameric pores. The resulting hypothetical models show a reduction in pore diameter and visual pore
540 collapse in both beta sheet peptide variants (R9P and R9P, R10L) **(Figure 8B and 8D)** but not with our
541 beta turn peptide variants (R11P and R10L, R11P) **(Figure 8C and 8E)**, where we found they maintain
542 pore integrity and diameter, only changing in peptide orientation within the pore. To understand the
543 structural instabilities leading to decreased pore formation we used GROMACs to observe changes in
544 the secondary structure in physiological salt conditions and within a lipid environment. When assessing
545 monomeric structural changes within salt conditions, we found the R9P beta sheet peptide variant loses
546 beta sheet structure early in the simulation while the R11P beta turn variant can maintain beta sheet
547 structure halfway through the simulation **(Figure 8G and 8H)**. The R9P, R10L beta sheet peptide variant
548 exhibits a much lower beta sheet character throughout the entirety of the simulation **(Figure 8I)**, while
549 the R10L, R11P beta turn peptide variant behaves much like R11P peptide variant **(Figure 8H and 8J)**.
550 These differences in monomeric behavior allowed us to hypothesize that perhaps pore formation is
551 hindered depending on at what point a variant loses its beta sheet character. When assessing the dimer
552 formation and stability in both salt and lipid environments we found overall the orientation of the dimer

553 changes with all variants, where the parental peptide dimerizes in parallel orientation and the variants in
554 anti-parallel orientation. In all the peptides maintained structural integrity in the lipid environment more
555 than the salt environment even at the beginning of the simulation (0 seconds) (**Figure 8K-8O**).
556 Furthermore, we found only the parental protegrin-1 dimer separated after 100 ns (**Figure 8K**). These
557 factors suggest strong dimerization may not be as important for pore formation with protegrin-1.
558
559 In conclusion, colistin and host defense peptides antimicrobial activity has been largely attributed to
560 charge, as peptides with a higher positive charge will be more attracted to the negatively charged
561 membrane. We show that with colistin-resistant *K. pneumoniae*, small changes in structure can impact
562 antimicrobial activity more than decreasing the peptide charge from +6 to +5. This work represents a step
563 towards understanding how to prevent activity loss due to colistin resistance membrane modifications
564 when designing therapeutics for *K. pneumoniae*.
565
566 **Acknowledgements**
567 This work is supported by the National Institutes of Health R00AI163295 to RMF; Cesar de la Fuente-
568 Nunez holds a Presidential Professorship at the University of Pennsylvania and acknowledges funding
569 from the Procter & Gamble Company, United Therapeutics, a BBRF Young Investigator Grant, the
570 Nemirovsky Prize, Penn Health-Tech Accelerator Award, and the Dean's Innovation Fund from the
571 Perelman School of Medicine at the University of Pennsylvania. Research reported in this publication
572 was supported by the Langer Prize (AIChE Foundation), the National Institute of General Medical
573 Sciences of the National Institutes of Health under award number R35GM138201, and the Defense
574 Threat Reduction Agency (DTRA; HDTRA11810041, HDTRA1-21-1-0014, and HDTRA1-23-1-0001). We
575 would like to thank Bryan Davies for his support and guidance on this work and Cory DuPais for teaching
576 Christina how to process the SLAY library from the Illumina sequencing reads.
577
578 **Declaration of Interests**

579 Cesar de la Fuente-Nunez provides consulting services to Invaio Sciences and is a member of the
580 Scientific Advisory Boards of Nowture S.L. and Phare Bio. The de la Fuente Lab has received research
581 funding or in-kind donations from United Therapeutics, Strata Manufacturing PJSC, and Procter &
582 Gamble, none of which were used in support of this work. Cesar de la Fuente-Nunez is on the Advisory
583 Board of *Cell Reports Physical Science*.
584
585 **Author Contributions**
586 R.M.F. conceived the idea and designed the experimentation. Initial library creation performed by N.R,
587 J.R, and R.M.F. Library analysis and direct cloning experiments performed by C.D. Antimicrobial activity
588 assessments and membrane analyses performed by S.A. and C.D. Molecular Dynamic simulations
589 performed by C.d.l.F.-N. and R.K. Biorender and AlphaFold images produced by C.D. Text was written
590 by R.M.F and C.D, and edits were discussed with C.d.l.F.-N., R.K. and J.R.
591
592 **Materials and Methods**
593
594 **Bacterial strains and peptides.**
595 All bacterial isolates used in this study are listed in **Supplemental Table S1**. The peptides used in this
596 study are listed in **Table 1** with their molecular weight, length, charge, and secondary structure. Pretegrin-
597 1 was ordered through Anaspec for the comparison to other host defense peptides in **Figure 2**. Arenicin
598 and Bac7(1-35) were purchased from Novopro because they were unavailable through Anaspec. For
599 consistency with our synthesized variants, protegrin-1 parent and peptide variants were ordered from
600 Novopro at >90% purity (https://www.novoprolabs.com) for comparing antimicrobial activity of amino acid
601 substitutions. All peptides were resuspended in ultra-purified water at 10 mg mL^{-1} and stored at -20 °C.
602
603 **Minimal inhibitory concentration assays**.

604 All minimal inhibitory concentration assays were performed using the broth dilution method in 96-well
605 plates with the peptides tested by serial diluting in 0.2% BSA 0.01% acetic acid solution [84]. Bacteria
606 were synchronized to mid-log phase and standardized to a final optical density 600nm (OD_{600}) of 0.001
607 in Mueller Hinton broth to yield ~$5x10^5$ CFU mL^{-1}. The assay incubated for 20 hours at 37 °C before
608 determining MICs. All MICs were performed in triplicate and repeated on separate days.
609
610 **RT-qPCR of *phoP* expression levels**
611 Each *K. pneumoniae* strain was grown overnight in LB broth. The following day each strain was
612 synchronized to exponential phase at 37°C for 3 hours. RNA was extracted after bacteria had been
613 synchronized for 3 hours at 37°C. Following hot phenol chloroform extraction previously described [50]
614 samples were resuspended in nuclease free H_20 and quantified by Nanodrop. RNA were aliquoted and
615 stored at -80 for RT-qPCR. Samples were reverse transcribed with SuperScript™ IV VILO™ Master Mix
616 (11756050, Invitrogen) following the manufacturer's instructions. RTqPCR was performed using
617 PowerUp™ SYBR™ Green Master Mix (A25742, Applied Biosystems) following the manufacturer's
618 instructions, and the QuantStudio 3 Real-Time PCR System (A28567, Applied Biosystems). Primers were
619 designed using Integrated DNA Technologies, Inc. (IDT)'s PrimerQuest tool (**Table S4**). Relative
620 expression levels were calculated using the 2-ΔΔCt method [49] with *rpoD* as housekeeping control.
621 Triplicate samples were used with error shown as ±SEM.
622
623 **Alpha Fold Images**
624 Images were initially prepared using Google Collab and this link
625 https://colab.research.google.com/github/sokrypton/ColabFold/blob/main/AlphaFold2.ipynb#scrollTo=1
626 1l8k--10q0C. Each sequence was input, and images were displayed using the ChimeraX visualizer.
627 Primary and secondary structures were overlayed and mutated amino acids are shown in red.
628
629 **Ramachandran Plot Generation**

630 Plots were generated by taking previously generated alpha fold files and displaying them with the
631 visualizing tool from UCSF chimera. Program can be accessed by utilizing this link
632 https://www.cgl.ucsf.edu/chimera/download.html. Plots were recolored and overlayed using Adobe
633 Photoshop.
634
635 **dmSLAY protegrin-1 analysis**
636 *dmSLAY creations and screening***.** The protegrin-1 deep mutational library was created as previously
637 described [60] and inserted into a tetracycline resistant pMMB67EH plasmid. The library was first
638 electroporated into *E. coli* C3020 and >150,000 colonies were collected. The library was then transformed
639 into *E. coli* SM10 λpir mating strain and >270,000 colonies were collected. Finally, conjugation was used
640 to introduce the library to *K. pneumoniae* MKP103 and ~200,000 colonies were collected. Samples were
641 frozen in glycerol stocks until library screening. Triplicate samples *K. pneumoniae* MKP103 harboring the
642 dmSLAY protegrin-1 library were thawed and back diluted to and OD_{600} 0.1 and grown for one hour. The
643 samples were then back diluted to OD_{600} 0.01 in 5 mL terrific broth (tryptone, yeast, potassium phosphate
644 dibasic, and glycerol) and triplicate samples were induced with 0.05 mM IPTG or uninduced (0mM IPTG)
645 for three hours shaking (220rpm) at 37 °C followed by, bacterial population collection and subsequent
646 plasmid extraction. Barcoded primers (Table S7) were used for PCR of the triplicate induced and
647 uninduced plasmid populations for amplification of the 240 bp amplicon for Illumina sequencing. One
648 lane of Illumina MiSeq run was used for amplicon coverage to allow for quantification and calculation of
649 log2 fold change between the induced and uninduced samples.
650
651 *Bioinformatic Analysis*. The next generation sequencing reads were process by having their forward and
652 reverse sequences merged together and adaptor sequences trimmed. For this we used a unique
653 modification of DESQ2, a package associated with R Studio, typically used to investigate the presence
654 of genes within a population. More specifically, we merged forward and reverse raw sequences from a

655 previously made protegrin-1 library, and adaptors were trimmed from both 5' and 3' end of the sequence.
656 Reads were counted and those occurring less than 50 times within the population were removed from
657 analysis to allow for the possibility of machine error. Translated DNA sequences were then compared to
658 the reads of the uninduced and induced populations using the Deseq2 package in R studio. To allow for
659 analysis of specifically those reads that did not kill the bacteria we eliminated reads with a log 2-fold
660 change below 0. From this data each amino acid mutation at each position in the total sequence variants
661 were counted to quantify their occurrence within the population of peptide variants.
662
663 **Direct Cloning of Peptide Variants**
664 Procedure adapted from previous methods [59]. Briefly, protegrin-1 parent plasmid was used as a
665 template for cloning via restriction enzymes on the broad host plasmid PMMB67EH with a tetracycline
666 resistance cassette. Sequences were cloned with peptide variant primers listed in **Table S5** with
667 homology to the tether sequence on the reverse primer. Restriction digestion was performed using KpmI
668 and SalI cut sites. Each peptide variant was then transformed into *E.coli C320* (NEB) electrocompetent
669 cells and sequence variants were confirmed by sanger sequencing. Plasmid was extracted from *E. coli*
670 using Qiagen mini-prep kit and electroporated into MKP103 for testing of antimicrobial activity with IPTG
671 induction.
672
673 **Surface display validation of mutations identified in library screen**
674 Growth curve procedure was adapted from previous methods [59]. Each *K. pneumoniae* strain with
675 plasmids harboring peptide variants and control plasmids listed in **Table S6**. were grown overnight in LB
676 broth and 1% glucose solution supplemented with 20µg/mL of tetracycline. The following day each strain
677 was synchronized to exponential phase at 37°C for 3 hours. At that time the strains were standardized to
678 an OD_{600} of 0.02. Bacterial strains were then added to culture tubes containing 2 mL LB, 0.5 mM IPTG,
679 and 20 µg mL^{-1} tetracycline and grown shaking (220rpm) at 37°C over the course of 4 hours. At 0, 1, 2,
680 and 4 hours 100 µL was removed from each culture tube and added to 900µL of 1XPBS for 1:10 serial

681 dilutions that were then plated on LB agar with 50 µg/mL tetracycline. All experiments were plated in
682 triplicate and incubated overnight at 37°C, and colony forming units per mL (CFU mL^{-1}) was calculated
683 with error reported as ±SEM.
684
685 **Outer Membrane Permeability**
686 Procedure adapted from previous methods [69-71] Each *K. pneumoniae* strain was grown overnight in
687 LB broth. The following day each strain was synchronized to exponential phase at 37°C for 3 hours. The
688 cells were harvested by centrifugation (3434 rcf for 10 min) washed twice with buffer A (5mM HEPES,
689 5mM glucose, pH 7.2) and resuspended in buffer A to an OD_{600} = 0.1. Then 100 µL Buffer A with 20 µM
690 NPN was added to 1000 µL washed cells in a clear-bottom black walled 96-well plate. Peptide was added
691 to a final concentration of 64 µg/mL and fluorescence was monitored at an excitation of 350nm and
692 emission of 420nm for 30 minutes at 3-minute intervals. The read form the no cell control wells were
693 removed from each treated well to normalize for background. All assays were performed in triplicate with
694 error reported as ±SEM.
695
696 **Membrane Depolarization**
697 The procedure used was adapted from a previous method [77]. Briefly, each *K. pneumoniae* strain was
698 grown overnight in LB broth. The following day each strain was synchronized to exponential phase at
699 37°C for 3 hours. The cells were harvested by centrifugation (3434 rcf for 10 min) washed twice with
700 buffer A (5mM HEPES, 5mM glucose, pH 7.2) and resuspended in buffer A and 100mM KCl to an OD_{600}
701 = 0.1, along with 20mM DiSC3 dye. Bacteria was added to clear-bottom black walled 96-well plate and
702 standardized for 30 minutes monitoring the florescence changes using a Biotech Synergy H1 plate reader
703 with fluorescence kinetic reads set with excitation of 622nm and emission of 670nm for 30 minutes at 2-
704 minute intervals. Peptide was then added to a final concentration of 64 µg mL^{-1} and fluorescence changes
705 were monitored for 30 minutes at 2-minute intervals using excitation of 622nm and emission of 670nm.
706 All assays were performed in triplicate with error reported as ±SEM.

Commented [RF1]: Rcf

707

708 **Inner Membrane Leakage**

709 The procedure used was adapted from a previous method [77, 78]. Each *K. pneumoniae* strain was
710 grown overnight in LB broth. The following day each strain was synchronized to exponential phase at
711 37°C for 3 hours. The cells were harvested by centrifugation (3434 rcf for 10 min) washed once with 0.1M
712 sodium phosphate buffer (26mM NaH_2PO_4, 77mM Na2HPO4, pH 7.4) and resuspended in 0.1M sodium
713 phosphate buffer to an OD_{600} = 0.1 along with 10mM ONPG. The peptide were then serially diluted in
714 sodium phosphate buffer in a clear-bottom walled black 96-well plate, bacteria were added, and
715 absorbance was read using a Biotech Synergy H1 plate reader at 410nm for 45 minutes with reads set
716 at 3-minute intervals.

717

718 **Molecular Dynamics Simulations**

719 GROMACs version 2025.0 located https://www.gromacs.org/index.html was used to perform the
720 analysis of the peptide variant monomers as well as dimers in both a saline medium (ionic strength:
721 0.15 M NaCl) and a general Gram-negative inner membrane environment located https://charmm-
722 gui.org/?doc=archive&lib=biomembrane. This analysis analyzed changes in peptide secondary structure
723 as well as fluctuations in center of mass and residue contacts with peptide variant dimers. Snapshots of
724 the peptide monomers were taken at 0ns, and peptide dimers were taken at 0 and 100ns to all for
725 visualization of structural changes in each subunit.

726

727 **Figure Legends**

728

729 **Figure 1. Multi-level analysis used to investigate how protegrin-1 can bypass colistin resistance**.
730 Our initial determination of MKP103 to have colistin-resistance yet has variable susceptibility to peptides
731 of different structural class was used to inform our deep mutation scanning utilizing a genetic screening
732 platform (bottom). We then investigate peptide variants mutated in different regions of the triple arginine
733 motif for changes in antimicrobial activity, disruption to both the outer and inner membrane (middle). We
734 ultimately use molecular modeling of peptides and octameric pores and combine this with molecular
735 dynamic simulations to assess peptide structure stability (top). Octameric, dimeric and monomeric
736 models were generated using Alpha Fold and Biorender was used for both vector production and for the
737 creation of the final figure.

738

739 **Figure 2. Host defense peptides do not equally bypass *K. pneumoniae* MKP103 PhoP acquired**
740 **polymyxin resistance**. This figure shows bacteria and peptide screening to determine ideal candidates
741 to investigate colistin resistance. Colistin and polymyxin B MICs against drug-resistant *K. pneumoniae*
742 MKP103, hypervirulent *K. pneumoniae* NTUH and KPPR1S, drug-resistant *K. pneumoniae* ATCC
743 700603, and type strain *K. pneumoniae* ATCC 13883 (bars) overlayed with the baseline *phoP* expression
744 in exponential growth phase, normalized to housekeeping gene *rpoD* and graphed in triplicate with error
745 shown as ±SEM (**Figure 2A**). Fold change in MICs between the *K. pneumoniae* MKP103 parental isolate
746 and a *⊿phoP* transposon mutant (KPNIH1_10030-701::T30) of polymyxin B (Poly-B), indolicidin (Indo),
747 Melittin (Mel), Arenicin (Are), protegrin-1 (PG-1), and CecropinA (Cec A) (**Figure 2B**). MIC assays were
748 performed in triplicate for the data shown. **Figures 2C-2E** show the Ramachandran plots depicting the
749 psi and phi angles of alpha helical peptides, beta sheet peptides, and extended/polyproline peptides,
750 respectively.

Commented [RF2]: Is this graph showing expression levels? 1.5? I think the right y-axis needs more appropriately labeled.

751

752 **Figure 3. Protegrin-1 deep mutational scanning library shows reveals charge and structure are**
753 **important for antimicrobial activity towards colistin-resistant *K. pneumoniae* MKP103**. This figure
754 shows the results of the initial SLAY screening as well as validation with direct cloning. **Figure 3A** is a
755 heat Map of SLAY library analysis showing the number of occurrences of the amino acid mutations in our
756 Illumina sequencing populations retained with induction with the parent peptide sequence on the y axis
757 and possible mutations on the x axis. White boxes denote mutations outside of the defined maximum
758 range of the heat map (20 occurrences). **Figure 3B** shows the Alpha Fold representation of protegrin-1
759 peptide with the mutations identified from the screen as outside of the defined maxima show with their
760 location highlighted in red and amino acid position number in parentheses. The amino acid mutations
761 denoted in blue text were cloned in the surface display system for validation by enumeration of CFU mL^{-}
762 ^{1} following IPTG plasmid induction over four hours with display of eighth the parent peptide protegrin-1,
763 uninduced plasmid control, and negative control 2xHA (**Figure 3C**) and peptide variants (**Figure 3D**)
764 identified in the screen. The surface display validation assays were performed in triplicate with error
765 shown.as as ±SEM.

766

767 **Figure 4. The arginine to proline mutation impedes antimicrobial activity only in the beta-sheet to**
768 **turn transition region of the protegrin-1 arginine loop.** The figures show MICs (μmol L^{-1}) of
769 synthesized peptide variants and fold-change in MICs between colistin-resistant *K. pneumoniae* MKP103
770 and transposon mutants lacking important LPS modifying genes. **Figure 4A** shows synthesized peptide
771 variants were tested against five colistin resistant clinical isolates. **Figure 4B** shows the fold change of
772 peptide MICs between the parental MKP103 and the *ΔphoP, ΔpagP, ΔpagL, ΔarnT,* and *ΔpmrB*
773 transposon mutants (mut/WT). Figure 4C and 4D shows the alanine and lysine peptide variants MICs
774 against the five colistin resistant clinical isolates and the fold change MICs between the parental MKP103

775 and transposon mutants. Lines are drawn on figures 4B and 4C follow the protegrin-1 parental peptide
776 fold-change in MIC for *ΔphoP* (blue) and downstream genetic mutants (red). Peptides were all tested at
777 a maximum concentration of 31 μmol L^{-1}. MIC assays were performed in triplicate for the data shown.

778

779 **Figure 5. Protegrin-1 double mutant variants with reduced charge display greater disruption of**
780 **colistin-resistant outer membrane.** Outer membrane fluorescence was monitored over 30 minutes with
781 peptide variants and controls carbenicillin and polymyxin B. **Figure 5A** shows *K. pneumoniae* MKP103
782 normalized NPN fluorescence after treatment with single peptide variants and Figure 5B shows the
783 double peptide variants. The NPN fluorescence for the *ΔphoP* transposon mutant is shown for peptide
784 variants in **Figures 5C and 5D**. Endpoint fluorescence reads with single peptide variant mutants with top
785 five colistin resistant MRSN isolates, parental MKP103, *ΔphoP, ΔpagP, ΔpagL, ΔarnT, and ΔpmrB*
786 transposon mutants is shown on **Figure 5E**, and double peptide variant mutants on **Figure 5F**. All
787 peptides and controls were tested in triplicate at a concentration of 31 μmol L^{-1} with error shown as
788 ±SEM.

789

790 **Figure 6. The arginine to proline mutation in the beta-sheet transition shows increased membrane**
791 **depolarization.** Membrane depolarization shows less active single peptide variant (R9P) depolarizing
792 more effectively than our more active single peptide variant (R11P). *K. pneumoniae* MKP103 tested with
793 single peptide variants (A) and double peptide variants (B). *ΔphoP* transposon mutant tested against
794 single peptide variants (C) and double peptide variants (D). Peptides were tested at a concentration of
795 31 μmol L^{-1} with error shown as ±SEM.

796 .

797

798 **Figure 7. The arginine to proline mutation in the beta-sheet transition limits cytosolic leakage in**
799 **single and double mutation variants.** Inner membrane leakage shows more active single peptide
800 variant (R11P) disrupting more effectively than our less active single peptide variants (R9P, R10L). *K.*
801 *pneumoniae* MKP103 tested with single peptide variants (A) and double peptide variants (B). *ΔphoP*
802 transposon mutant tested against single peptide variants (C) and double peptide variants (D). Peptides
803 were tested at a concentration of 31 μmol L^{-1} with error shown as ±SEM.

804

805 **Figure 8. Molecular modeling shows octameric pore collapse and loss of beta sheet character in**
806 **beta sheet peptide variants.** Peptide variants are shown modeled as octameric pores in **Figure 8A-8E**
807 using AlphaFold2 and visualized using ChimeraX for parent protegrin-1 (**A**), R9P (**B**), R11P (**C**),
808 RR910PL (**D**) and RR1011LP (**E**). Amino acid sequences were aligned in the N to C termini direction.
809 **Figures 8F-8J** show monomeric peptide variants simulated using GROMACs and observed for changes
810 in secondary structure parent protegrin-1 (**F**), R9P (**G**), R11P (b), R9P, R10L (**I**) and R10L, R11P (**J**).
811 The heat map labels show the color coding for B = Beta Bridge, T =Turn, E = Extended Conformation, C
812 = Coil peptide structural components. **Figures 8K-8O** show dimeric peptide variants simulated using
813 GROMACs in both a salt box (0.15M NaCl at 310K) (top) and a general Gram-negative inner membrane
814 (bottom). Snapshots are shown for parent protegrin-1 (**K**), R9P (**L**), R11P (**M**), R9P, R10L (**N**) and R10L,
815 R11P (**O**) at 0 and 100ns for both simulated environments.

816

817 **Tables.**

818 **Table 1. Host defense peptides tested for antimicrobial activity towards *K. pneumoniae* MKP103**
819 **and MKP103 *ΔphoP* mutant.**
820

Name	AA sequence	MW (g/mol)	Charge	Secondary structure
Il-37[a]	LLGDFFRKSKEKIGKEFKRIVQRIKDFLRNLVPRTES	4492.34	+6	Alpha helix
Indolicidin[a]	ILPWKWPWWPWRR - NH2	1906.28	+4	extended
Protegrin-1[a]	RGGRLCYCRRRFCVCVGR - NH2	2003.48	+6	Beta sheet
Arenicin[b]	RWCVYAYVRVRGVLVRYRRCW-OH	2758.2	+6	Beta sheet
Cecropin[a]	KWKLFKKIEKVGQNIRDGIIKAGPAVAVVGQATQIAK-NH2	4004.10	+7	Alpha helix
Melittin[a]	GIGAVLKVLTTGLPALISWIKRKRQQ-NH2	2846.7	+6	Alpha helix
Bac7 (1-35)[b]	RRIRPRPPRLPRPRPRPLPFPRPGPRPIPRPLPFP-NH2	4206.16	+11	polyproline

821
822 [a] Peptide ordered from Anaspec
823 [b] Peptide ordered from Novopro

824 **Table 2. Occurrence of amino acid mutations in the peptide variant sequences lacking**
825 **antimicrobial activity.**
826

Amino Acid Mutation	Amino Acid Class Change	Number of Occurrences
F12L	non-polar to non-polar	834
G2R	non-polar to positive-charge	316
R10L*	positive-charge to non-polar	299
R9P*	positive-charge to non-polar	295
L5I	non-polar to non-polar	218
C6S	non-polar to polar	35
C13S	non-polar to polar	27
C15R	non-polar to positive-charge	22
G3R	non-polar to positive-charge	21
F12Y	non-polar to polar	21

827 *Amino acid mutations found together in 89% occurrences
828
829

830 **Table 3. Synthesized Peptide Variants.**

Name	Amino Acid Sequence	MW (g/mol)	Charge
PG-1 parent	RGGRLCYCRRRFCVCVGR	2160.63	+6
R9P	RGGRLCYCPRRFCVCVGR	2101.56	+5
R10L	RGGRLCYCRLRFCVCVGR	2117.60	+5
R11P	RGGRLCYCRRPFCVCVGR	2101.56	+5
RR910PL	RGGRLCYCPLRFCVCVGR	2058.53	+4
RR1011LP	RGGRLCYCRLPFCVCVGR	2058.53	+4
R9A	RGGRLCYCARRFCVCVGR	2075.52	+5
R11A	RGGRLCYCRRAFCVCVGR	2075.52	+5
R9K	RGGRLCYCKRRFCVCVGR	2132.62	+6
R11K	RGGRLCYCRRKFCVCVGR	2132.62	+6

831
832
833

834 **Table 4. Minimum inhibitory concentration of protegrin-1 and peptide variants towards *K.***
835 ***pneumoniae* MKP103 and transposon mutants.**
836

Peptide Variant	MIC (μmol L^{-1} / μg mL^{-1})					
	MKP103 WT	***ΔphoP***	***ΔpagP***	***ΔpagL***	***ΔarnT***	***ΔpmrB***
PG-1 parent	3.70/8	0.12/0.25	3.70/8	3.70/8	3.70/8	3.70/8
R9P	15.23/32	0.48/1	15.23/32	15.23/32	15.23/32	15.23/32
R10L	15.11/32	1.89/4	15.11/32	15.11/32	7.56/16	7.56/16
R11P	3.81/8	0.95/2	0.95/2	0.95/2	1.90/4	1.90/4
RR1011LP	31.09/64	0.97/2	15.55/32	15.55/32	15.55/32	15.55/32
RR910PL	31.09/64	3.89/8	31.09/64	31.09/64	31.09/64	31.09/64
R9A	15.41/32	0.96/2	1.93/4	3.85/8	1.93/4	3.85/8
R11A	15.41/32	0.48/1	0.96/2	0.96/2	0.96/2	1.93/4
R9K	3.75/8	0.47/1	0.94/2	0.94/2	0.94/2	0.94/2
R11K	7.50/16	0.47/1	0.94/2	0.94/2	0.94/2	0.94/2

837

838 **References**

839 1. Paczosa, M.K. and J. Mecsas, *Klebsiella pneumoniae: Going on the Offense with a Strong*
840 *Defense.* Microbiol Mol Biol Rev, 2016. **80**(3): p. 629-61.
841 2. Asokan, S., et al., *Klebsiella pneumoniae: A growing threat in the era of antimicrobial resistance.*
842 The Microbe, 2025. **7**: p. 100333.
843 3. Navon-Venezia, S., K. Kondratyeva, and A. Carattoli, *Klebsiella pneumoniae: a major worldwide*
844 *source and shuttle for antibiotic resistance.* FEMS Microbiol Rev, 2017. **41**(3): p. 252-275.
845 4. Shah, A.A., et al., *Emerging challenges in Klebsiella pneumoniae: Antimicrobial resistance and*
846 *novel approach.* Microbial Pathogenesis, 2025. **202**: p. 107399.
847 5. Reynolds, D., et al., *The threat of multidrug-resistant/extensively drug-resistant Gram-negative*
848 *respiratory infections: another pandemic.* Eur Respir Rev, 2022. **31**(166).
849 6. Antimicrobial Resistance, C., *Global burden of bacterial antimicrobial resistance in 2019: a*
850 *systematic analysis.* Lancet, 2022. **399**(10325): p. 629-655.
851 7. Petrosillo, N., F. Taglietti, and G. Granata, *Treatment Options for Colistin Resistant Klebsiella*
852 *pneumoniae: Present and Future.* J Clin Med, 2019. **8**(7).
853 8. Wyres, K.L., M.M.C. Lam, and K.E. Holt, *Population genomics of Klebsiella pneumoniae.* Nat Rev
854 Microbiol, 2020. **18**(6): p. 344-359.
855 9. Sati, H., et al., *The WHO Bacterial Priority Pathogens List 2024: a prioritisation study to guide*
856 *research, development, and public health strategies against antimicrobial resistance.* Lancet
857 Infect Dis, 2025.
858 10. Mondal, A.H., et al., *A Review on Colistin Resistance: An Antibiotic of Last Resort.*
859 Microorganisms, 2024. **12**(4).
860 11. Rojas, L.J., et al., *Colistin Resistance in Carbapenem-Resistant Klebsiella pneumoniae:*
861 *Laboratory Detection and Impact on Mortality.* Clin Infect Dis, 2017. **64**(6): p. 711-718.
862 12. van Duin, D. and Y. Doi, *Outbreak of Colistin-Resistant, Carbapenemase-Producing Klebsiella*
863 *pneumoniae: Are We at the End of the Road?* J Clin Microbiol, 2015. **53**(10): p. 3116-7.
864 13. Luterbach, C.L., et al., *Transmission of Carbapenem-Resistant Klebsiella pneumoniae in US*
865 *Hospitals.* Clin Infect Dis, 2023. **76**(2): p. 229-237.
866 14. Horvath, M., et al., *Virulence Characteristics and Molecular Typing of Carbapenem-Resistant*
867 *ST15 Klebsiella pneumoniae Clinical Isolates, Possessing the K24 Capsular Type.* Antibiotics
868 (Basel), 2023. **12**(3).
869 15. Marsh, J.W., et al., *Evolution of Outbreak-Causing Carbapenem-Resistant Klebsiella pneumoniae*
870 *ST258 at a Tertiary Care Hospital over 8 Years.* mBio, 2019. **10**(5).
871 16. Chen, L., et al., *Epidemic Klebsiella pneumoniae ST258 Is a Hybrid Strain.* mBio, 2014. **5**(3): p.
872 10.1128/mbio.01355-14.
873 17. Bogdanovich, T., et al., *Colistin-resistant, Klebsiella pneumoniae carbapenemase (KPC)-*
874 *producing Klebsiella pneumoniae belonging to the international epidemic clone ST258.* Clin
875 Infect Dis, 2011. **53**(4): p. 373-6.
876 18. Lapp, Z., et al., *Fitness barriers to spread of colistin resistance overcome by first establishing*
877 *niche in patients with enhanced colistin exposure.* medRxiv, 2021: p. 2021.06.11.21258758.
878 19. Pitt, M.E., et al., *Octapeptin C4 and polymyxin resistance occur via distinct pathways in an*
879 *epidemic XDR Klebsiella pneumoniae ST258 isolate.* J Antimicrob Chemother, 2019. **74**(3): p.
880 582-593.

881 20. Arena, F., et al., *Colistin Resistance Caused by Inactivation of the MgrB Regulator Is Not*
882 *Associated with Decreased Virulence of Sequence Type 258 KPC Carbapenemase-Producing*
883 *Klebsiella pneumoniae.* Antimicrob Agents Chemother, 2016. **60**(4): p. 2509-12.
884 21. Diani, E., et al., *Colistin: Lights and Shadows of an Older Antibiotic.* Molecules, 2024. **29**(13).
885 22. Khondker, A. and M.C. Rheinstädter, *How do bacterial membranes resist polymyxin antibiotics?*
886 Communications Biology, 2020. **3**(1): p. 77.
887 23. Hamel, M., J.M. Rolain, and S.A. Baron, *The History of Colistin Resistance Mechanisms in*
888 *Bacteria: Progress and Challenges.* Microorganisms, 2021. **9**(2).
889 24. Yu, Z., et al., *Antibacterial mechanisms of polymyxin and bacterial resistance.* Biomed Res Int,
890 2015. **2015**: p. 679109.
891 25. Simpson, B.W. and M.S. Trent, *Pushing the envelope: LPS modifications and their consequences.*
892 Nat Rev Microbiol, 2019. **17**(7): p. 403-416.
893 26. Bray, A.S., et al., *MgrB-Dependent Colistin Resistance in Klebsiella pneumoniae Is Associated*
894 *with an Increase in Host-to-Host Transmission.* mBio, 2022. **13**(2): p. e03595-21.
895 27. Janssen, A.B., et al., *Evolution of Colistin Resistance in the Klebsiella pneumoniae Complex*
896 *Follows Multiple Evolutionary Trajectories with Variable Effects on Fitness and Virulence*
897 *Characteristics.* Antimicrob Agents Chemother, 2020. **65**(1).
898 28. Li, L., et al., *Roles of two-component regulatory systems in Klebsiella pneumoniae: Regulation of*
899 *virulence, antibiotic resistance, and stress responses.* Microbiol Res, 2023. **272**: p. 127374.
900 29. Kim, S.J., et al., *Roles of crrAB two-component regulatory system in Klebsiella pneumoniae:*
901 *growth yield, survival in initial colistin treatment stage, and virulence.* Int J Antimicrob Agents,
902 2024. **63**(1): p. 107011.
903 30. Arroyo Luis, A., et al., *The pmrCAB Operon Mediates Polymyxin Resistance in Acinetobacter*
904 *baumannii ATCC 17978 and Clinical Isolates through Phosphoethanolamine Modification of*
905 *Lipid A.* Antimicrobial Agents and Chemotherapy, 2011. **55**(8): p. 3743-3751.
906 31. Lee, K.K., et al., *Heterogeneous efflux pump expression underpins phenotypic resistance to*
907 *antimicrobial peptides*. 2024, eLife Sciences Publications, Ltd.
908 32. MacNair, C.R., et al., *Overcoming mcr-1 mediated colistin resistance with colistin in combination*
909 *with other antibiotics.* Nat Commun, 2018. **9**(1): p. 458.
910 33. Brogden, K.A., *Antimicrobial peptides: pore formers or metabolic inhibitors in bacteria?* Nat Rev
911 Microbiol, 2005. **3**(3): p. 238-50.
912 34. Sengupta, D., et al., *Toroidal pores formed by antimicrobial peptides show significant disorder.*
913 Biochimica et Biophysica Acta (BBA) - Biomembranes, 2008. **1778**(10): p. 2308-2317.
914 35. Zhang, Q.Y., et al., *Antimicrobial peptides: mechanism of action, activity and clinical potential.*
915 Mil Med Res, 2021. **8**(1): p. 48.
916 36. Hancock, R.E. and A. Rozek, *Role of membranes in the activities of antimicrobial cationic*
917 *peptides.* FEMS Microbiol Lett, 2002. **206**(2): p. 143-9.
918 37. Fleeman, R.M. and B.W. Davies, *Polyproline Peptide Aggregation with Klebsiella pneumoniae*
919 *Extracellular Polysaccharides Exposes Biofilm Associated Bacteria.* Microbiol Spectr, 2022. **10**(2):
920 p. e0202721.
921 38. Fleeman, R.M., et al., *Defining principles that influence antimicrobial peptide activity against*
922 *capsulated Klebsiella pneumoniae.* Proc Natl Acad Sci U S A, 2020. **117**(44): p. 27620-27626.
923 39. El-Sayed Ahmed, M.A.E., et al., *Colistin and its role in the Era of antibiotic resistance: an*
924 *extended review (2000-2019).* Emerg Microbes Infect, 2020. **9**(1): p. 868-885.

40. Lei, J., et al., *The antimicrobial peptides and their potential clinical applications.* Am J Transl Res, 2019. **11**(7): p. 3919-3931.
41. Drayton, M., et al., *Host Defense Peptides: Dual Antimicrobial and Immunomodulatory Action.* Int J Mol Sci, 2021. **22**(20).
42. Bader, M.W., et al., *Recognition of Antimicrobial Peptides by a Bacterial Sensor Kinase.* Cell, 2005. **122**(3): p. 461-472.
43. Wu, K.-M., et al., *Genome Sequencing and Comparative Analysis of Klebsiella pneumoniae NTUH-K2044, a Strain Causing Liver Abscess and Meningitis.* Journal of Bacteriology, 2009. **191**(14): p. 4492-4501.
44. Walker Kimberly, A., et al., *A Klebsiella pneumoniae Regulatory Mutant Has Reduced Capsule Expression but Retains Hypermucoviscosity.* mBio, 2019. **10**(2): p. 10.1128/mbio.00089-19.
45. Rasheed, J.K., et al., *Characterization of the Extended-Spectrum β-Lactamase Reference Strain, Klebsiella pneumoniae K6 (ATCC 700603), Which Produces the Novel Enzyme SHV-18.* Antimicrobial Agents and Chemotherapy, 2000. **44**(9): p. 2382-2388.
46. Cowan, S.T., et al., *A classification of the Klebsiella group.* J Gen Microbiol, 1960. **23**: p. 601-12.
47. Ramage, B., et al., *Comprehensive Arrayed Transposon Mutant Library of Klebsiella pneumoniae Outbreak Strain KPNIH1.* J Bacteriol, 2017. **199**(20).
48. Snitkin, E.S., et al., *Tracking a hospital outbreak of carbapenem-resistant Klebsiella pneumoniae with whole-genome sequencing.* Sci Transl Med, 2012. **4**(148): p. 148ra116.
49. Livak, K.J. and T.D. Schmittgen, *Analysis of relative gene expression data using real-time quantitative PCR and the 2(-Delta Delta C(T)) Method.* Methods, 2001. **25**(4): p. 402-8.
50. Aiba, H., S. Adhya, and B. de Crombrugghe, *Evidence for two functional gal promoters in intact Escherichia coli cells.* J Biol Chem, 1981. **256**(22): p. 11905-10.
51. Mardirossian, M., et al., *The Host Antimicrobial Peptide Bac71-35 Binds to Bacterial Ribosomal Proteins and Inhibits Protein Synthesis.* Chemistry & Biology, 2014. **21**(12): p. 1639-1647.
52. Barlow, D.J. and J.M. Thornton, *Helix geometry in proteins.* Journal of Molecular Biology, 1988. **201**(3): p. 601-619.
53. Hauser, K., et al., *Characterization of Biomolecular Helices and Their Complementarity Using Geometric Analysis.* J Chem Inf Model, 2017. **57**(4): p. 864-874.
54. Hollingsworth, S.A. and P.A. Karplus, *A fresh look at the Ramachandran plot and the occurrence of standard structures in proteins.* Biomol Concepts, 2010. **1**(3-4): p. 271-283.
55. Bolintineanu, D.S., V. Vivcharuk, and Y.N. Kaznessis, *Multiscale models of the antimicrobial peptide protegrin-1 on gram-negative bacteria membranes.* Int J Mol Sci, 2012. **13**(9): p. 11000-11011.
56. Fahrner, R.L., et al., *Solution structure of protegrin-1, a broad-spectrum antimicrobial peptide from porcine leukocytes.* Chem Biol, 1996. **3**(7): p. 543-50.
57. Steinberg, D.A., et al., *Protegrin-1: a broad-spectrum, rapidly microbicidal peptide with in vivo activity.* Antimicrob Agents Chemother, 1997. **41**(8): p. 1738-42.
58. Tachi, Y., S.G. Itoh, and H. Okumura, *Molecular dynamics simulations of amyloid-beta peptides in heterogeneous environments.* Biophys Physicobiol, 2022. **19**: p. 1-18.
59. Tucker, A.T., et al., *Discovery of Next-Generation Antimicrobials through Bacterial Self-Screening of Surface-Displayed Peptide Libraries.* Cell, 2018. **172**(3): p. 618-628 e13.
60. Randall, J.R., et al., *Deep mutational scanning and machine learning uncover antimicrobial peptide features driving membrane selectivity.* Res Sq, 2023.

969 61. Rodziewicz-Motowidlo, S., et al., *Antimicrobial and conformational studies of the active and*
970 *inactive analogues of the protegrin-1 peptide.* FEBS J, 2010. **277**(4): p. 1010-22.
971 62. Mohanram, H. and S. Bhattacharjya, *Cysteine deleted protegrin-1 (CDP-1): Anti-bacterial*
972 *activity, outer-membrane disruption and selectivity.* Biochimica et Biophysica Acta (BBA) -
973 General Subjects, 2014. **1840**(10): p. 3006-3016.
974 63. Martin, M.J., et al., *A panel of diverse Klebsiella pneumoniae clinical isolates for research and*
975 *development.* Microb Genom, 2023. **9**(5).
976 64. Bishop, R.E., *The lipid A palmitoyltransferase PagP: molecular mechanisms and role in bacterial*
977 *pathogenesis.* Mol Microbiol, 2005. **57**(4): p. 900-12.
978 65. Brett, P.J., D. DeShazer, and D.E. Woods, *Burkholderia thailandensis sp. nov., a Burkholderia*
979 *pseudomallei-like species.* Int J Syst Bacteriol, 1998. **48 Pt 1**: p. 317-20.
980 66. Jacobs Anna, C., et al., *AB5075, a Highly Virulent Isolate of Acinetobacter baumannii, as a Model*
981 *Strain for the Evaluation of Pathogenesis and Antimicrobial Treatments.* mBio, 2014. **5**(3): p.
982 10.1128/mbio.01076-14.
983 67. Jensen, K.F., *The Escherichia coli K-12 "wild types" W3110 and MG1655 have an rph frameshift*
984 *mutation that leads to pyrimidine starvation due to low pyrE expression levels.* J Bacteriol, 1993.
985 **175**(11): p. 3401-7.
986 68. Minogue, T.D., et al., *Complete Genome Assembly of Escherichia coli ATCC 25922, a Serotype O6*
987 *Reference Strain.* Genome Announc, 2014. **2**(5).
988 69. Loh, B., C. Grant, and R.E. Hancock, *Use of the fluorescent probe 1-N-phenylnaphthylamine to*
989 *study the interactions of aminoglycoside antibiotics with the outer membrane of Pseudomonas*
990 *aeruginosa.* Antimicrob Agents Chemother, 1984. **26**(4): p. 546-51.
991 70. Muheim, C., et al., *Increasing the permeability of Escherichia coli using MAC13243.* Sci Rep,
992 2017. **7**(1): p. 17629.
993 71. Richard, C.S.M., et al., *Outer Membrane Integrity-Dependent Fluorescence of the Japanese Eel*
994 *UnaG Protein in Live Escherichia coli Cells.* Biosensors (Basel), 2023. **13**(2).
995 72. Rizzetto, G., et al., *Protegrin-1 and Analogues Against Acinetobacter baumannii: A Narrative*
996 *Review.* Pharmaceuticals (Basel), 2025. **18**(3).
997 73. Huang, H.W., *DAPTOMYCIN, its membrane-active mechanism vs. that of other antimicrobial*
998 *peptides.* Biochimica et Biophysica Acta (BBA) - Biomembranes, 2020. **1862**(10): p. 183395.
999 74. Spindler, E.C., et al., *Deciphering the mode of action of the synthetic antimicrobial peptide*
1000 *Bac8c.* Antimicrob Agents Chemother, 2011. **55**(4): p. 1706-16.
1001 75. Mihaylova-Garnizova, R., et al., *Antimicrobial Peptides Derived from Bacteria: Classification,*
1002 *Sources, and Mechanism of Action against Multidrug-Resistant Bacteria.* Int J Mol Sci, 2024.
1003 **25**(19).
1004 76. Xiao, B., et al., *Unlocking the Potential of Antimicrobial Peptides: Cutting-Edge Advances and*
1005 *Therapeutic Potential in Combating Bacterial Keratitis.* Bioconjug Chem, 2025. **36**(3): p. 311-
1006 331.
1007 77. Moller, A.M., et al., *Common and varied molecular responses of Escherichia coli to five different*
1008 *inhibitors of the lipopolysaccharide biosynthetic enzyme LpxC.* J Biol Chem, 2024. **300**(4): p.
1009 107143.
1010 78. Gravel, J., C. Paradis-Bleau, and A.R. Schmitzer, *Adaptation of a bacterial membrane*
1011 *permeabilization assay for quantitative evaluation of benzalkonium chloride as a membrane-*
1012 *disrupting agent.* MedChemComm, 2017. **8**(7): p. 1408-1413.

1013 79. Nielsen, J.E., et al., *Self-Assembly of Antimicrobial Peptoids Impacts Their Biological Effects on*
1014 *ESKAPE Bacterial Pathogens.* ACS Infect Dis, 2022. **8**(3): p. 533-545.
1015 80. Ferreira, A.F.L., et al., *Defensins identified through molecular de-extinction.* Cell Reports Physical
1016 Science, 2024. **5**(9): p. 102193.
1017 81. Pogozheva, I.D., et al., *Comparative Molecular Dynamics Simulation Studies of Realistic*
1018 *Eukaryotic, Prokaryotic, and Archaeal Membranes.* J Chem Inf Model, 2022. **62**(4): p. 1036-
1019 1051.
1020 82. Saxena, D., et al., *Tackling the outer membrane: facilitating compound entry into Gram-*
1021 *negative bacterial pathogens.* npj Antimicrobials and Resistance, 2023. **1**(1): p. 17.
1022 83. Trimble, M.J., et al., *Polymyxin: Alternative Mechanisms of Action and Resistance.* Cold Spring
1023 Harb Perspect Med, 2016. **6**(10).
1024 84. Wiegand, I., K. Hilpert, and R.E.W. Hancock, *Agar and broth dilution methods to determine the*
1025 *minimal inhibitory concentration (MIC) of antimicrobial substances.* Nature Protocols, 2008.
1026 **3**(2): p. 163-175.
1027
1028

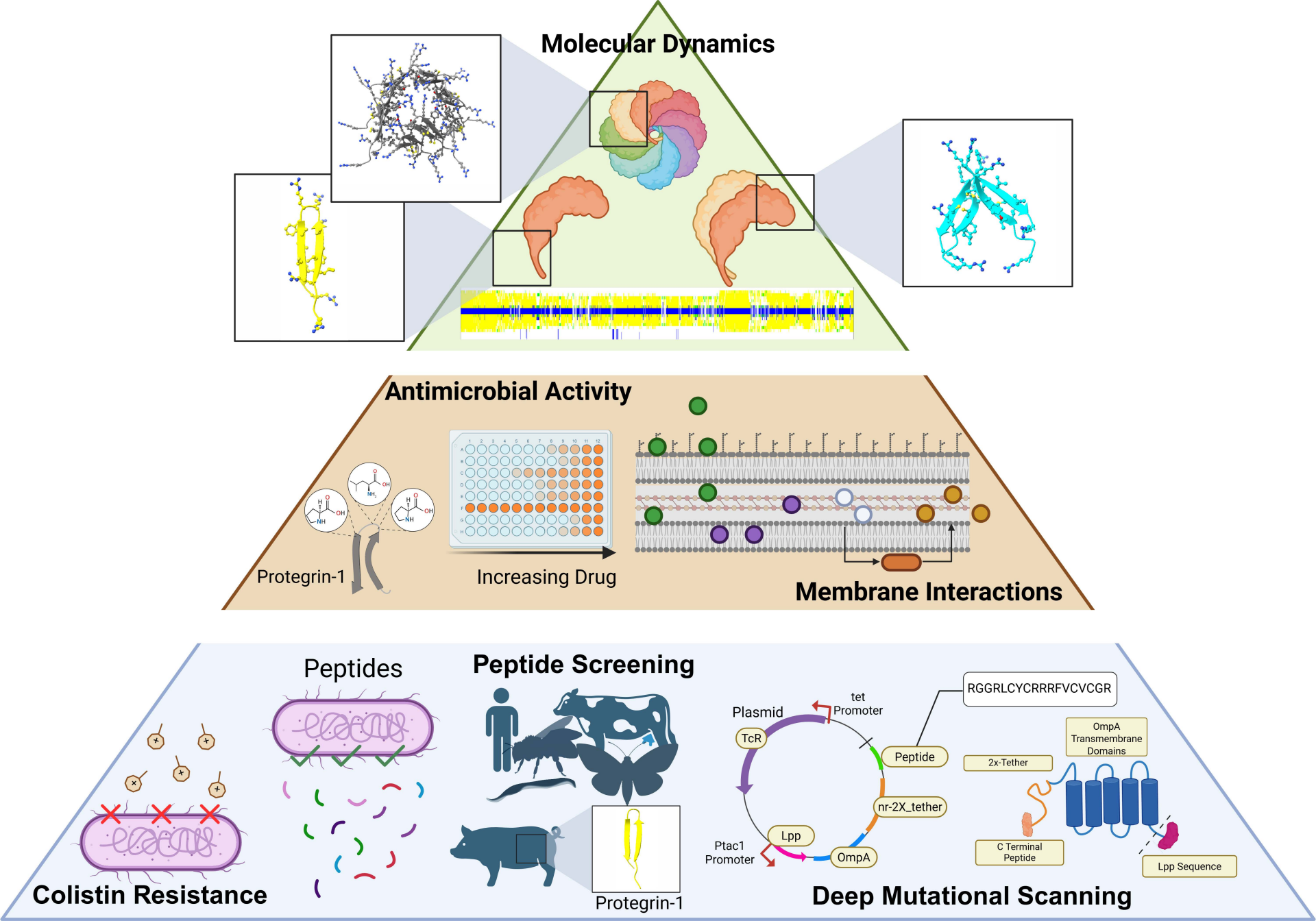
Molecular Dynamics
Antimicrobial Activity
Protegrin-1
Increasing Drug
Membrane Interactions
Peptides
Peptide Screening
Colistin Resistance
Protegrin-1
Plasmid
tet
Promoter
TcR
Peptide
nr-2X_tether
Lpp
OmpA
Ptac1
Promoter
RGGRLCYCRRRFVCVCGR
OmpA
Transmembrane
Domains
2x-Tether
C Terminal
Peptide
Lpp Sequence
Deep Mutational Scanning

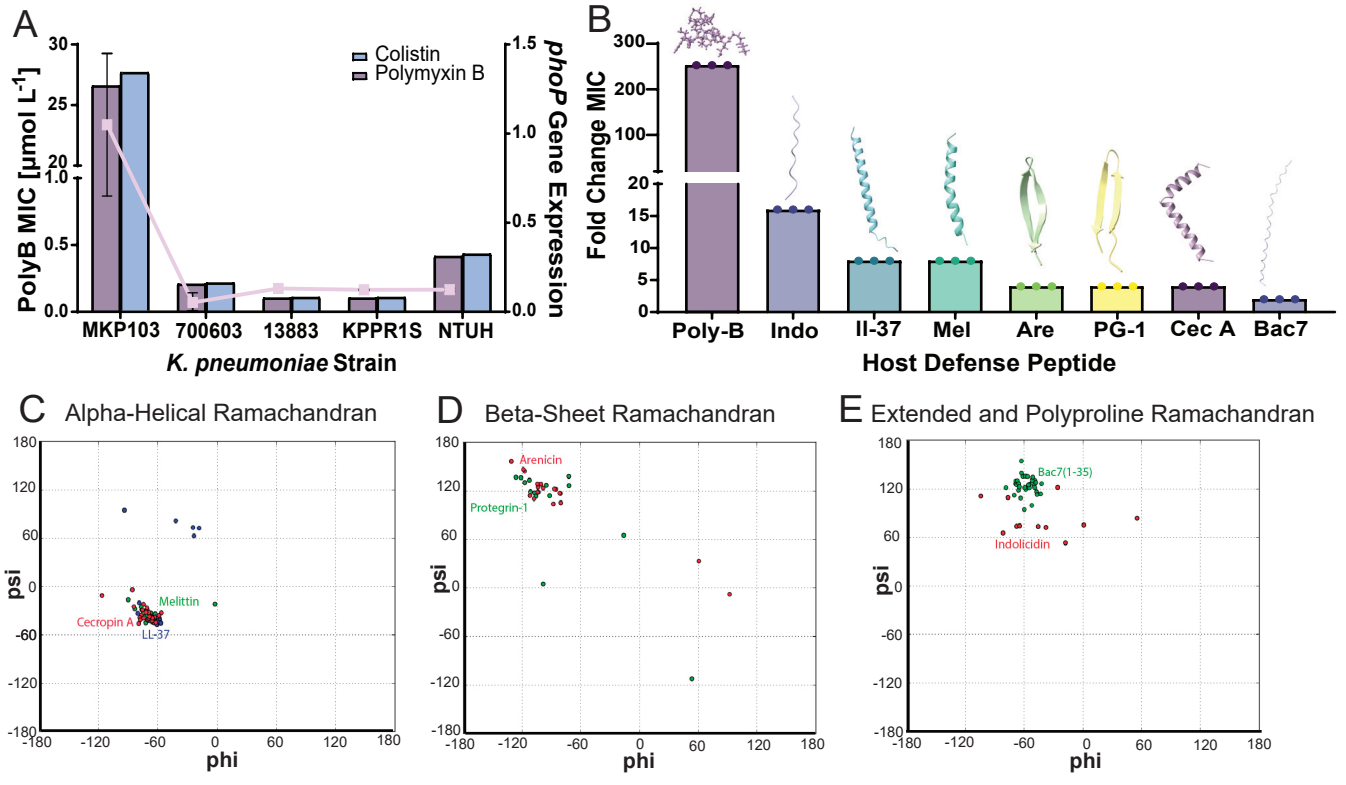
A
Colistin
Polymyxin B
PolyB MIC [μmol L-1]
phoP Gene Expression
MKP103
700603
13883
KPPR1S
NTUH
K. pneumoniae Strain
B
Fold Change MIC
Poly-B
Indo
II-37
Mel
Are
PG-1
Cec A
Bac7
Host Defense Peptide
C Alpha-Helical Ramachandran
Melittin
Cecropin A
LL-37
psi
phi
D Beta-Sheet Ramachandran
Arenicin
Protegrin-1
psi
phi
E Extended and Polyproline Ramachandran
Bac7(1-35)
Indolicidin
psi
phi

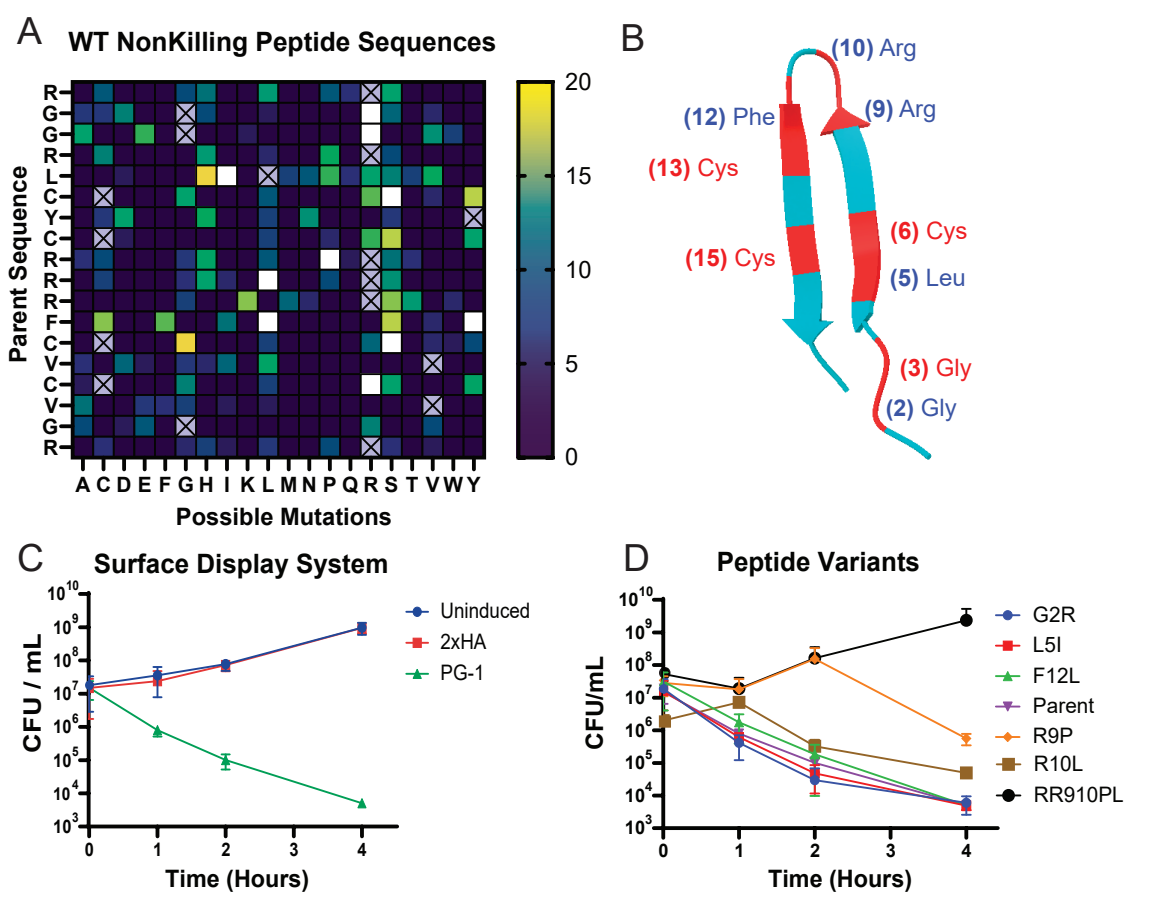
A
WT NonKilling Peptide Sequences
Parent Sequence
R G G R L C Y C R R R F C V C V G R
A C D E F G H I K L M N P Q R S T V W Y
Possible Mutations
20
15
10
5
0
B
(10) Arg
(9) Arg
(12) Phe
(13) Cys
(6) Cys
(15) Cys
(5) Leu
(3) Gly
(2) Gly
C
Surface Display System
CFU / mL
Time (Hours)
Uninduced
2xHA
PG-1
D
Peptide Variants
CFU/mL
Time (Hours)
G2R
L5I
F12L
Parent
R9P
R10L
RR910PL

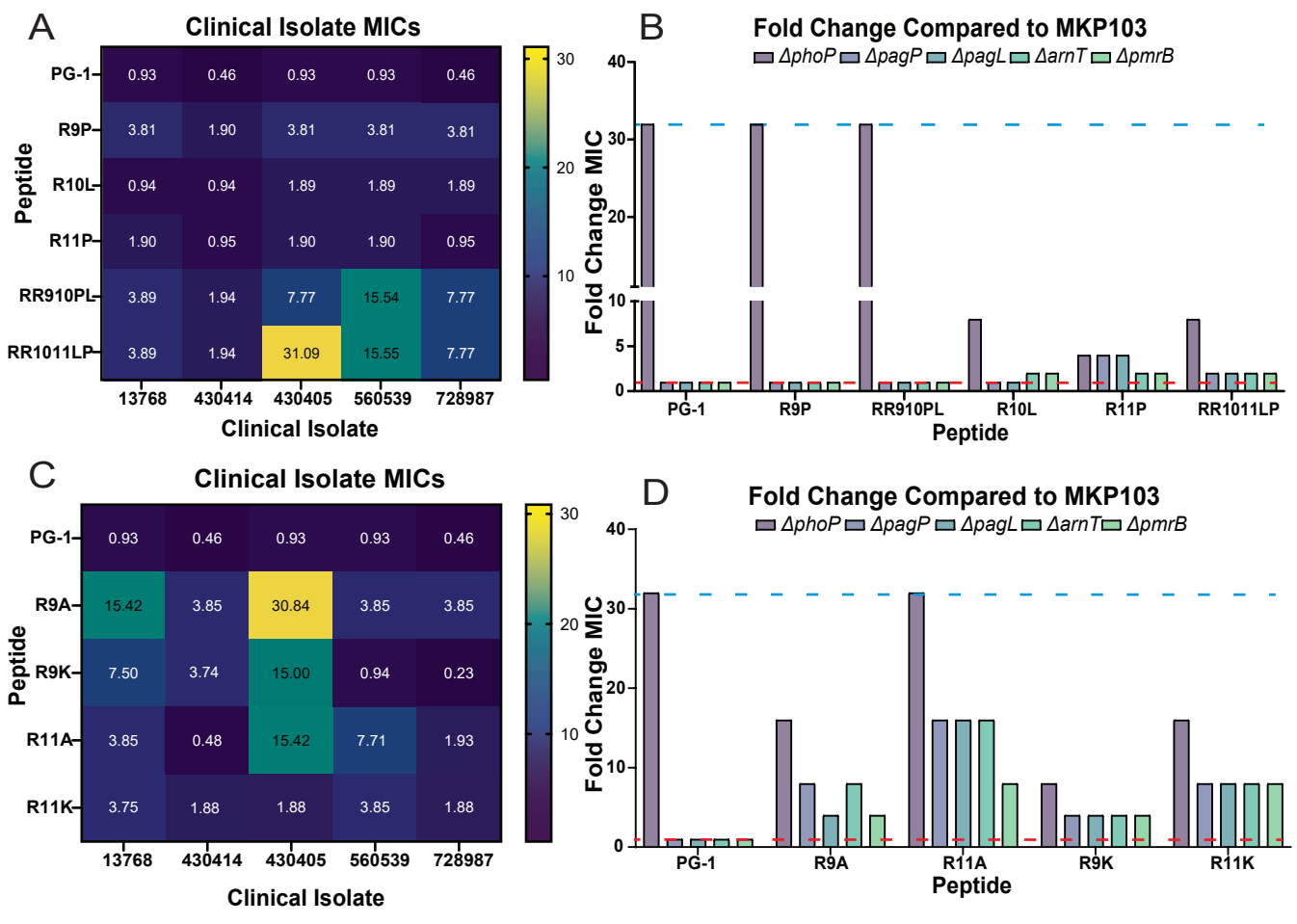
A
Clinical Isolate MICs
Peptide
PG-1
R9P
R10L
R11P
RR910PL
RR1011LP
0.93 0.46 0.93 0.93 0.46
3.81 1.90 3.81 3.81 3.81
0.94 0.94 1.89 1.89 1.89
1.90 0.95 1.90 1.90 0.95
3.89 1.94 7.77 15.54 7.77
3.89 1.94 31.09 15.55 7.77
13768 430414 430405 560539 728987
Clinical Isolate
30
20
10
B
Fold Change Compared to MKP103
ΔphoP ΔpagP ΔpagL ΔarnT ΔpmrB
Fold Change MIC
40
30
20
10
5
0
PG-1 R9P RR910PL R10L R11P RR1011LP
Peptide
C
Clinical Isolate MICs
Peptide
PG-1
R9A
R9K
R11A
R11K
0.93 0.46 0.93 0.93 0.46
15.42 3.85 30.84 3.85 3.85
7.50 3.74 15.00 0.94 0.23
3.85 0.48 15.42 7.71 1.93
3.75 1.88 1.88 3.85 1.88
13768 430414 430405 560539 728987
Clinical Isolate
30
20
10
D
Fold Change Compared to MKP103
ΔphoP ΔpagP ΔpagL ΔarnT ΔpmrB
Fold Change MIC
40
30
20
10
0
PG-1 R9A R11A R9K R11K
Peptide

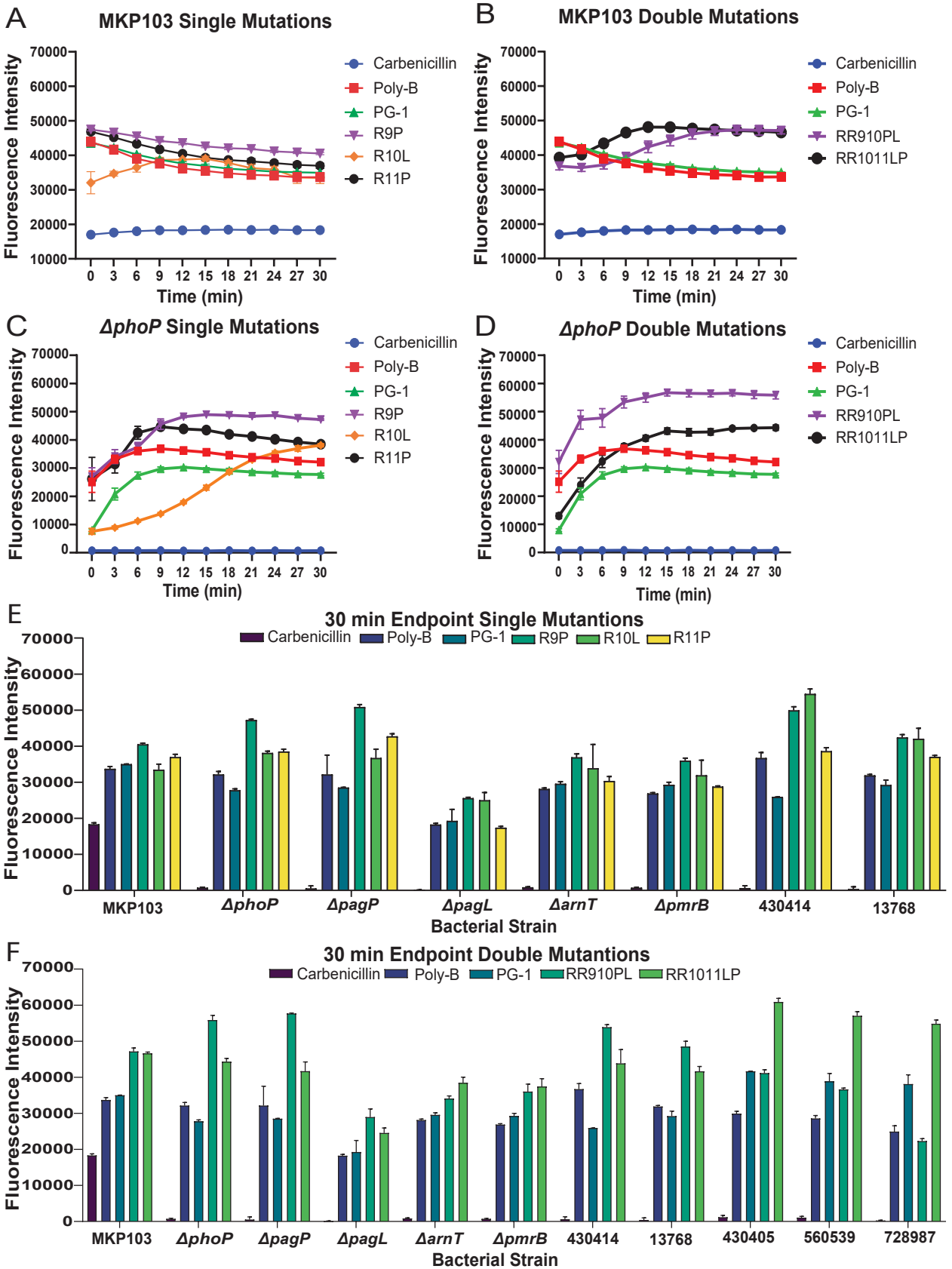
A
MKP103 Single Mutations
Fluorescence Intensity
Time (min)
Carbenicillin
Poly-B
PG-1
R9P
R10L
R11P
B
MKP103 Double Mutations
Fluorescence Intensity
Time (min)
Carbenicillin
Poly-B
PG-1
RR910PL
RR1011LP
C
ΔphoP Single Mutations
Fluorescence Intensity
Time (min)
Carbenicillin
Poly-B
PG-1
R9P
R10L
R11P
D
ΔphoP Double Mutations
Fluorescence Intensity
Time (min)
Carbenicillin
Poly-B
PG-1
RR910PL
RR1011LP
E
30 min Endpoint Single Mutantions
Carbenicillin
Poly-B
PG-1
R9P
R10L
R11P
Fluorescence Intensity
MKP103
ΔphoP
ΔpagP
ΔpagL
ΔarnT
ΔpmrB
430414
13768
Bacterial Strain
F
30 min Endpoint Double Mutantions
Carbenicillin
Poly-B
PG-1
RR910PL
RR1011LP
Fluorescence Intensity
MKP103
ΔphoP
ΔpagP
ΔpagL
ΔarnT
ΔpmrB
430414
13768
430405
560539
728987
Bacterial Strain

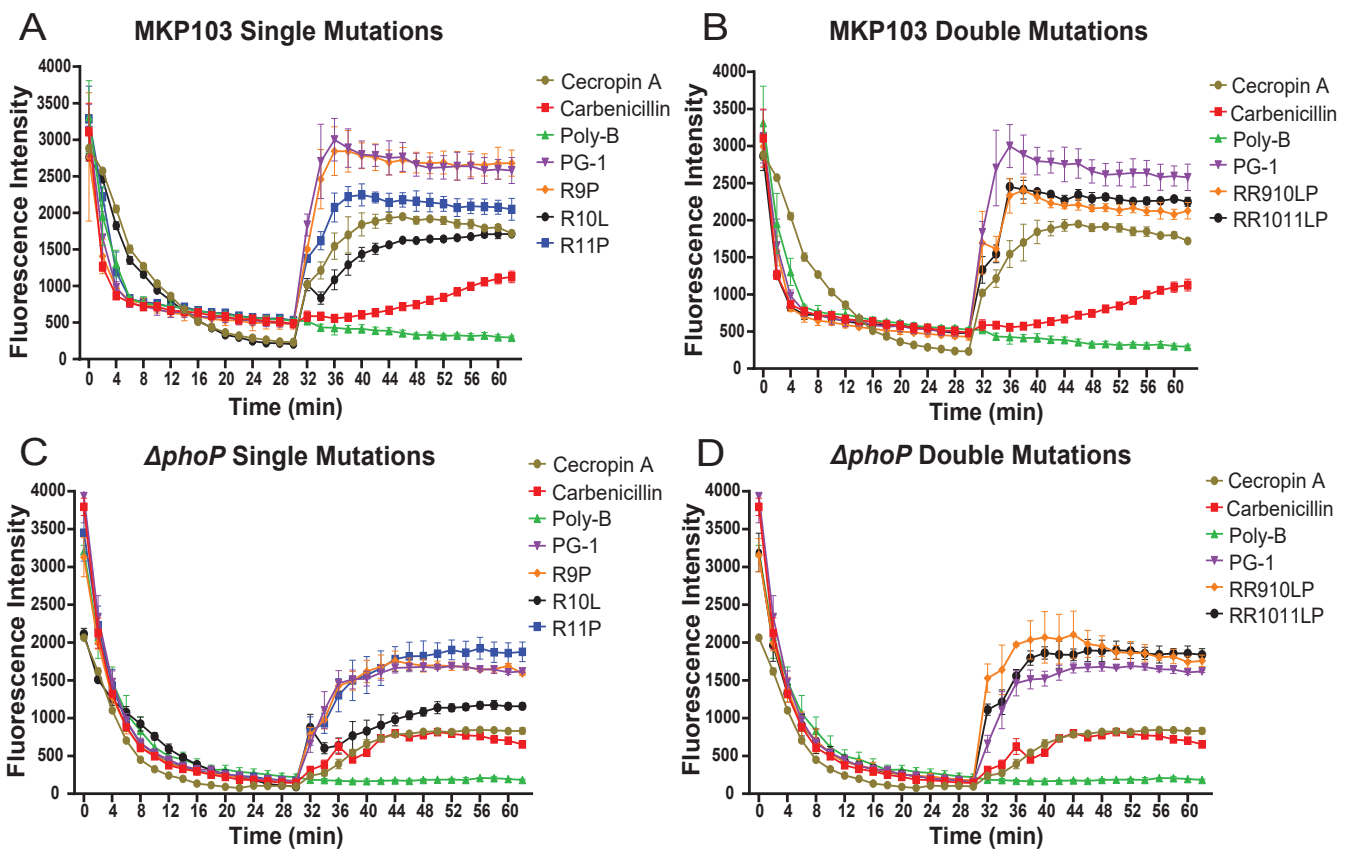
A
MKP103 Single Mutations
Fluorescence Intensity
Time (min)
Cecropin A
Carbenicillin
Poly-B
PG-1
R9P
R10L
R11P
B
MKP103 Double Mutations
Fluorescence Intensity
Time (min)
Cecropin A
Carbenicillin
Poly-B
PG-1
RR910LP
RR1011LP
C
ΔphoP Single Mutations
Fluorescence Intensity
Time (min)
Cecropin A
Carbenicillin
Poly-B
PG-1
R9P
R10L
R11P
D
ΔphoP Double Mutations
Fluorescence Intensity
Time (min)
Cecropin A
Carbenicillin
Poly-B
PG-1
RR910LP
RR1011LP

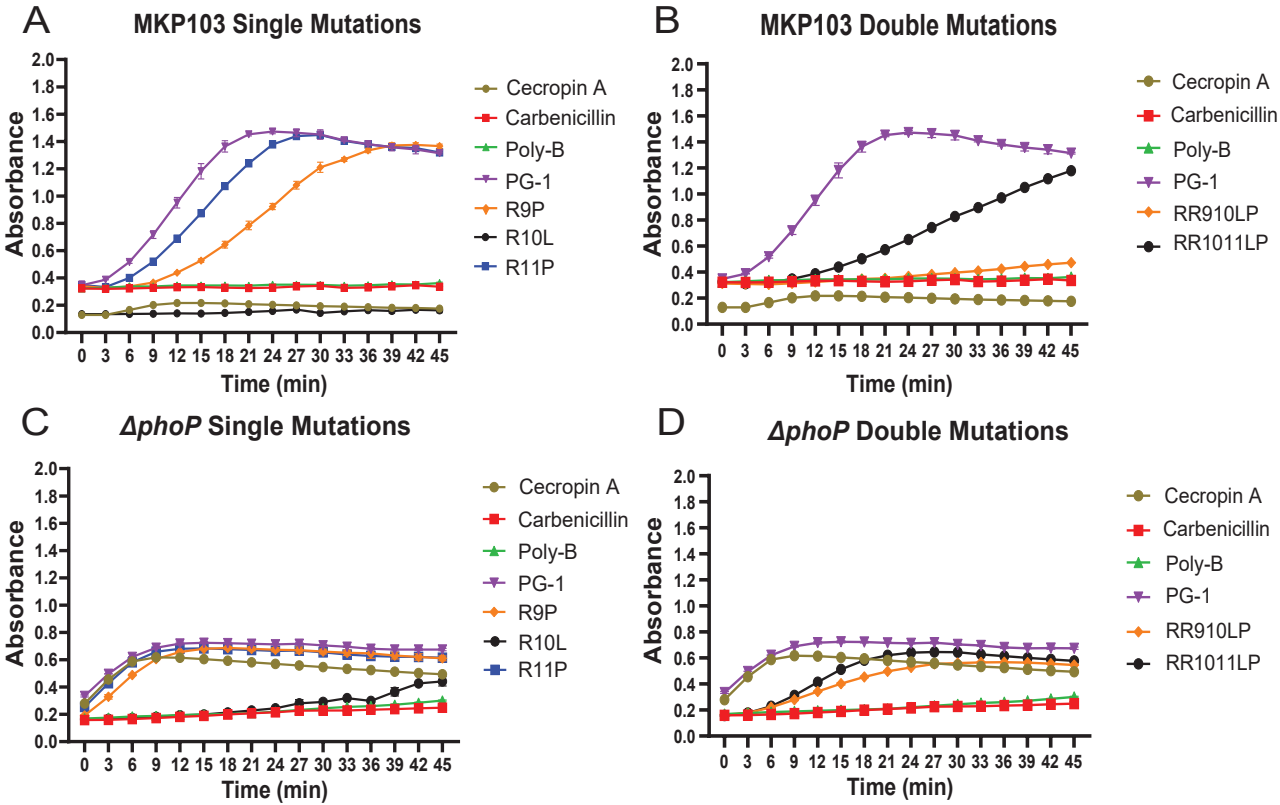
A
MKP103 Single Mutations
Absorbance
Time (min)
Cecropin A
Carbenicillin
Poly-B
PG-1
R9P
R10L
R11P
B
MKP103 Double Mutations
Absorbance
Time (min)
Cecropin A
Carbenicillin
Poly-B
PG-1
RR910LP
RR1011LP
C
ΔphoP Single Mutations
Absorbance
Time (min)
Cecropin A
Carbenicillin
Poly-B
PG-1
R9P
R10L
R11P
D
ΔphoP Double Mutations
Absorbance
Time (min)
Cecropin A
Carbenicillin
Poly-B
PG-1
RR910LP
RR1011LP

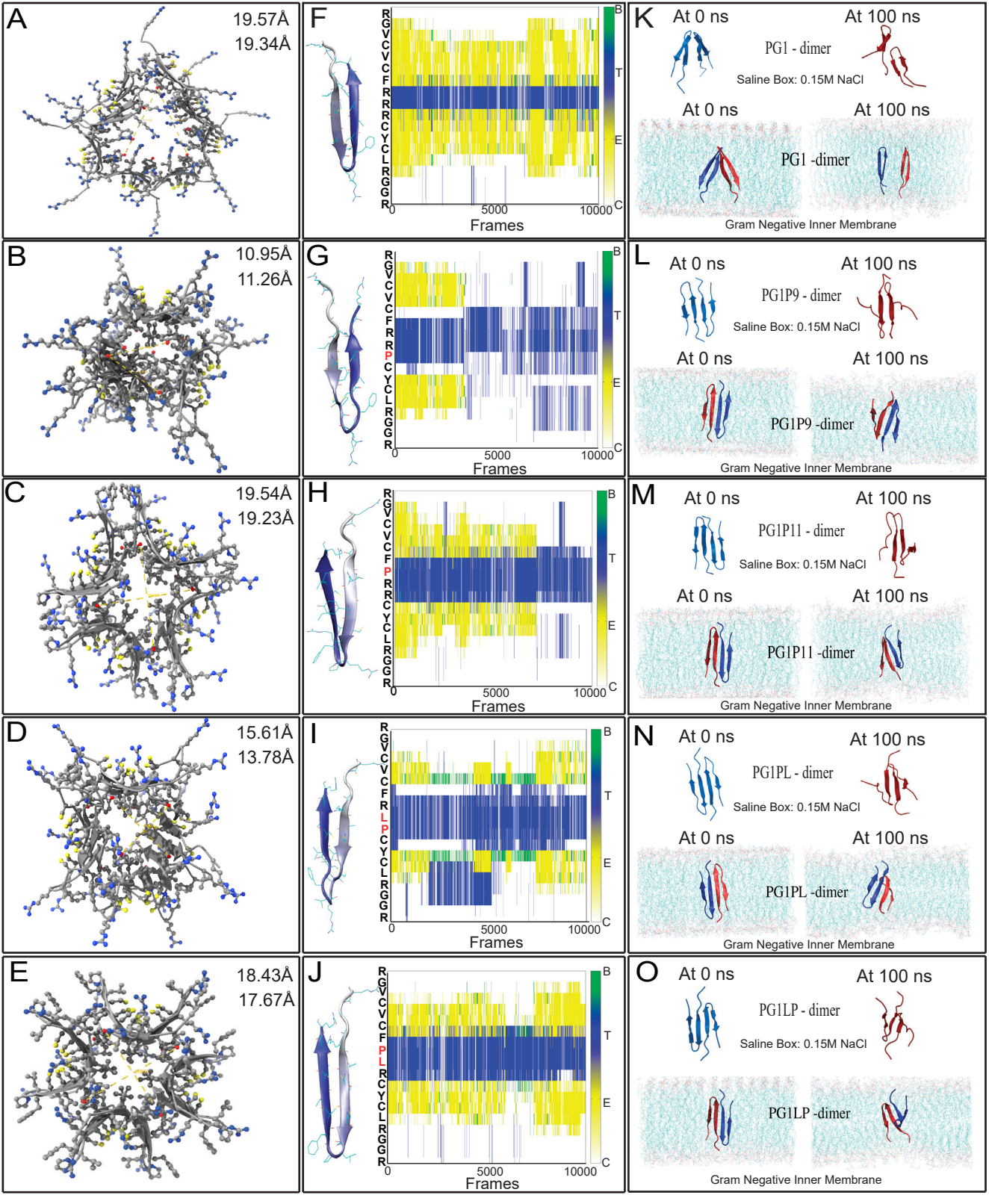
A
19.57Å
19.34Å
B
10.95Å
11.26Å
C
19.54Å
19.23Å
D
15.61Å
13.78Å
E
18.43Å
17.67Å
F
G
H
I
J
R G V C V C F R R R C Y C L R G G R
R G V C V C F R R P C Y C L R G G R
R G V C V C F P R R C Y C L R G G R
R G V C V C F R L P C Y C L R G G R
R G V C V C F P L R C Y C L R G G R
B
T
E
C
0
5000
10000
Frames
K
L
M
N
O
At 0 ns
At 100 ns
PG1 - dimer
PG1 -dimer
PG1P9 - dimer
PG1P9 -dimer
PG1P11 - dimer
PG1P11 -dimer
PG1PL - dimer
PG1PL -dimer
PG1LP - dimer
PG1LP -dimer
Saline Box: 0.15M NaCl
Gram Negative Inner Membrane